Cellular/Molecular

Selective Functional Interactions between Excitatory and Inhibitory Cortical Neurons and Differential Contribution to Persistent Activity of the Slow Oscillation

Babak Tahvildari, Markus Wölfel, Alvaro Duque, and David A. McCormick
Department of Neurobiology and Kavli Institute for Neuroscience, Yale University School of Medicine, New Haven, Connecticut 06510

The neocortex depends upon a relative balance of recurrent excitation and inhibition for its operation. During spontaneous Up states, cortical pyramidal cells receive proportional barrages of excitatory and inhibitory synaptic potentials. Many of these synaptic potentials arise from the activity of nearby neurons, although the identity of these cells is relatively unknown, especially for those underlying the generation of inhibitory synaptic events. To address these fundamental questions, we developed an *in vitro* submerged slice preparation of the mouse entorhinal cortex that generates robust and regular spontaneous recurrent network activity in the form of the slow oscillation. By performing whole-cell recordings from multiple cell types identified with green fluorescent protein expression and electrophysiological and/or morphological properties, we show that distinct functional subpopulations of neurons exist in the entorhinal cortex, with large variations in contribution to the generation of balanced excitation and inhibition during the slow oscillation. The most active neurons during the slow oscillation are excitatory pyramidal and inhibitory fast spiking interneurons, receiving robust barrages of both excitatory and inhibitory synaptic potentials. Weak action potential activity was observed in stellate excitatory neurons and somatostatin-containing interneurons. In contrast, interneurons containing neuropeptide Y, vasoactive intestinal peptide, or the 5-hydroxytryptamine (serotonin) 3a receptor, were silent. Our data demonstrate remarkable functional specificity in the interactions between different excitatory and inhibitory cortical neuronal subtypes, and suggest that it is the large recurrent interaction between pyramidal neurons and fast spiking interneurons that is responsible for the generation of persistent activity that characterizes the depolarized states of the cortex.

Introduction

The cerebral cortex is characterized by a densely interconnected network of excitatory principal neurons and local inhibitory interneurons that influences all cortical functions, from spontaneous rhythmic oscillations to extraction of sensory information. Because of strong intermingling of recurrent excitatory and inhibitory pathways, there is a proportional balance of excitation and inhibition in network activity, which is responsible for a wide range of phenomena, such as the generation of slow (e.g., $<$1 Hz) and fast (e.g., 30–80 Hz) oscillations (Traub et al., 1996; Shu et al., 2003), rapid onset and offset dynamics (Shadlen and Newsome, 1994), broad variability in spike timing (Mainen and Sejnowski, 1995; Wehr and Zador, 2003), and persistent activity without epileptogenic or other maladaptive forms of discharge (Wang, 2001; McCormick et al., 2003).

One prototypical example of activity generated by cortical recurrent networks is the slow oscillation (Steriade et al., 1993, 2001; Sanchez-Vives and McCormick, 2000). The cortical slow oscillation is characterized by 0.5–3 s periods of persistent activity (Up states) that are generated by the dynamic interaction of recurrent excitatory and inhibitory connections. These Up states are regularly interrupted by periods of network silence (Down states). Not only does the slow oscillation occur during slow wave sleep and anesthesia but also during periods of drowsiness or inattentiveness (Petersen et al., 2003). Transition to the awake, attentive state results in the selective loss of Down states, such that the membrane potential of cortical pyramidal cells resembles a prolonged Up-like state, implying that the neural mechanisms of the Up state may be in many ways similar to those of the waking, attentive state (Steriade et al., 2001; Destexhe et al., 2007).

While the recurrent excitation of cortical pyramidal cells during the Up state appears to originate from other pyramidal neurons, the source of the robust inhibitory potentials is less known, although fast-spiking (FS) GABAergic interneurons are one likely input, since these are highly active (Steriade et al., 2001; Cunningham et al., 2006; Haider et al., 2006; Fanselow and Connors, 2010). The cerebral cortex contains a wide variety of inhibitory interneurons that can be segregated based upon somatic-dendritic morphology, intrinsic membrane properties, calcium-binding protein or peptide content, axonal projections, and postsynaptic effects, among other features (Gonchar et al., 2007;

Received Feb. 24, 2012; revised June 7, 2012; accepted June 25, 2012.

Author contributions: B.T. and D.A.M. designed research; B.T., M.W., A.D., and D.A.M. performed research; B.T. analyzed data; B.T. and D.A.M. wrote the paper.

This work was supported by the National Institutes of Health and the Kavli Institute for Neuroscience at Yale. B.T. was an awardee of The Robert Leet and Clara Guthrie Patterson Trust Postdoctoral Fellowship, Bank of America, Trustee. We thank Edward Zagha, Matthew McGinley, and Amanda Casale for comments on this manuscript.

Correspondence should be addressed to David A. McCormick, Department of Neurobiology and Kavli Institute for Neuroscience, Yale University School of Medicine, 333 Cedar Street, New Haven, CT 06510. E-mail: david.mccormick@yale.edu.

DOI:10.1523/JNEUROSCI.1181–12.2012

 0270-6474/12/3212165-15$15.00/0

Ascoli et al., 2008; Uematsu et al., 2008; Xu et al., 2010; Kubota et al., 2011; Rudy et al., 2011).

To examine how different types of inhibitory interneurons behave during the recurrent activity of the Up state, we developed an *in vitro* slice preparation of the mouse entorhinal cortex that generates a robust spontaneous slow oscillation in submersion-style recording chamber in physiological saline. Surprisingly, our recordings reveal that, of five subgroups, fast-spiking, somatostatin (SOM), neuropeptide Y (NPY), vasoactive intestinal peptide (VIP), and 5HT3a receptor-containing interneurons (5HTR3a), which collectively can account for the large majority of GABAergic cells in layers 2/3 (Gonchar et al., 2007; Uematsu et al., 2008; Rudy et al., 2011), only the fast-spiking interneurons are highly active during the Up state. These data reveal a remarkable specificity within functional inhibitory networks and suggest that fast-spiking neurons are the primary source of IPSPs during ongoing recurrent cortical activity and are primarily responsible for maintaining the balance of excitation and inhibition that is critical to proper cortical function.

Materials and Methods

Animals. All animal handling and experimental procedures were approved by the Institutional Animal Care and Use Committee at Yale University in accordance with National Institutes of Health guidelines for ethical treatment of animals. Five different mouse lines expressing either enhanced green fluorescent protein (EGFP) or humanized *Renilla* green fluorescent protein (hrGFP) or Zs-Green in a subpopulation of interneurons were used in this study. The mouse lines were as follows: (1) regulator of calcineurin 2 (RCan2) [STOCK Tg (Rcan2-EGFP) EI79Gsat; stock number 010591-UCD; GENSAT], (2) GIN (Oliva et al., 2000) [FVB-Tg(GadGFP) 45704 Swn/J; stock number 003718; The Jackson Laboratory], (3) NPY [B6.FVB-Tg(Npy-hrGFP)1Lowl/J; stock number 006417; The Jackson Laboratory], (4) VIP [STOCK Viptm1(cre)Zjh/J; stock number 010908; The Jackson Laboratory], and (5) 5-hydroxytryptamine (serotonin) receptor 3a (5HTR3a) [STOCK Tg(Htr3a-EGFP) DP271 Gsat; stock number 010546-UCD; GENSAT].

All five lines of mice, except GIN and VIP, were hemizygous. Homozygous males and females of GIN mice were bred to generate homozygous offspring. For the VIP mouse line, we used the homozygous mouse line expressing Cre under the VIP promoter. Males and females were crossed with homozygous floxed ZsGreen1 mice [B6.Cg-Gt(ROSA)26Sortm6 (CAG-ZsGreen1)Hze/J; stock number 007906; The Jackson Laboratory] for ZsGreen1 expression restricted to VIP cells. For the other mouse lines (RCan2, 5HTR3a, and NPY), hemizygous males were bred with wild-type females of the same background (Swiss Webster wild-type females for RCan2 and 5HTR3a mouse lines, and C57BL/6J for NPY mouse line). Pups expressing EGFP/hrGFP/Zs-Green were distinguished from wild-type pups by exposing their skull to fluorescent illumination with an appropriate filter under a dissecting microscope (Discovery.V8; Nikon) at an early age (postnatal days 0–2).

Preparation of brain slices. We prepared near horizontal slices (~15° off the horizontal plane; see Fig. 1*A*) of the entorhinal cortex (EC). The EC was chosen for study because of its ability to robustly generate the slow oscillation in slices of mouse cortex. Examination of other cortical areas (e.g., somatosensory, visual, and prefrontal) revealed only sparse Up-state activity in our recording setups (Fanselow and Connors, 2010). Male or female transgenic mice (12–18 postnatal days) were deeply anesthetized with sodium pentobarbital (150 mg/kg) and killed through decapitation. The cerebellum and the brainstem were removed with a knife cut while the brain was in the cranium. The forebrain was gently removed and placed in ice-cold (~4°C) cutting solution containing the following (in mM): 85 NaCl, 75 sucrose, 2.5 KCl, 25 $NaHCO_3$, 1.25 NaH_2PO_4, 3.5 $MgSO_4$, 0.5 $CaCl_2$, 10 glucose, 3 *myo*-inositol, 3 Na-pyruvate, 0.5 L-ascorbic acid, and aerated with 95% O_2, 5% CO_2 to a final pH of 7.4. The blocked brain was placed on its dorsal surface in a custom knife guidance tool. A coronal cut was performed to remove the rostral half of the brain (see Fig. 1*A*, cut 1). The brain was placed on the rostral cut surface (with occipital cortex facing upward) into the same custom knife guidance tool. The dorsal surface of the neocortex was then trimmed with a knife cut ~15° (posterior toward anterior) with respect to the horizontal plane (see Fig. 1*A*, cut 2). The trimmed brain was then glued, with the dorsal surface of the cut facing down, to an ice-cold vibratome stage (VT1000 S; Leica Microsystems). Slices of the EC and adjacent cortical regions were cut (320 μm thickness) in ice-cold cutting solution (Fig. 1*A*). The sections were placed in an incubator at ~35°C for 30 min in the cutting solution, and were then incubated for at least an additional 30 min in a holding chamber at room temperature containing the following (in mM): 125 NaCl, 3 KCl, 25 $NaHCO_3$, 1.25 NaH_2PO_4, 2.0 $MgSO_4$, 2.0 $CaCl_2$, 10 glucose, 3 *myo*-inositol, 3 Na-pyruvate, 0.5 L-ascorbic acid.

Recording procedures and drugs. For recordings, a slice was transferred to a submersion style recording chamber located on the stage of an upright, fixed-stage microscope (Axioskop; Carl Zeiss Microscopy) equipped with a water-immersion objective (40×), a near-infrared charge-coupled device camera, and a mercury short arc lamp. To perfuse both the upper and lower surface of the brain tissue with physiological solution, slices were placed between two nylon nets (model: SHD-27LP/15 and SHD-41/15; Warner Instruments). Flow rate of well oxygenated solution was kept high (3–5 ml/min) so as to maintain neuronal health throughout the slice (Hájos et al., 2009). For recordings, the extracellular medium had the same composition as the incubation solution except for the concentrations of calcium and magnesium, which were reduced to 1.2 and 1.0 mM, respectively. Stellate and pyramidal cells were distinguished based on the shape, size, and position of their somata within layers 2 and 3 of the EC as seen under infrared–differential interference contrast (IR-DIC) microscopy. Interneurons were visualized and detected using the epifluorescent light in combination with DIC. All recordings were performed at ~32°C.

Simultaneous multiple-unit (MU) and whole-cell recordings (50–200 μm apart) were performed using a MultiClamp 700B amplifier (Molecular Devices). Borosilicate glass electrodes (World Precision Instruments) were pulled on a Brown Flaming puller (model P-97; Sutter Instrument) for recordings. For MU recordings, glass electrodes (1–2 MΩ) were backfilled with the extracellular solution and the electrical signal was bandpass filtered between 300 Hz and 2 kHz and digitized at 2 kHz with either a Digidata 1320 interface (Molecular Devices) or the Spike2 data acquisition system (Cambridge Electronic Design).

Current-clamp whole-cell recordings were obtained with 4–7 MΩ tip resistance micropipettes filled with the following (in mM): 130 K-gluconate, 7 KCl, 10 HEPES, 4 Mg-ATP, 0.3 Na-GTP, 10 Na-phosphocreatine, and 0.4% (w/v) biocytin, pH 7.25 adjusted with KOH (pipette solution osmolarity was ~300 mOsm). After establishing a gigaohm seal, the cell membrane was ruptured by application of gentle negative pressure. The apparent input resistance, membrane time constant, and discharge behavior of the recorded neurons were examined through the injection of a family of depolarizing and hyperpolarizing (500 ms) current pulses during the silent state of neural network activity. Up and Down states were examined at several different membrane potentials (from approximately −100 to approximately −50 mV) through the intracellular injection of DC.

For voltage-clamp recordings, the micropipettes (4–7 MΩ tip resistance) were filled with the following (in mM): 130 cesium-gluconate, 3.5 CsCl, 10 HEPES, 4 Mg-ATP, 0.3 Na-GTP, 10 Na-phosphocreatine, 3.5 QX-314-Cl (Tocris Bioscience), 1 EGTA, and 0.4% (w/v) biocytin, pH 7.25, adjusted with CsOH. Cesium-gluconate and QX-314-Cl were included to reduce and block voltage-dependent potassium and sodium currents, as well as the h-current and $GABA_B$ synaptic potentials (Connors and Prince, 1982; Nathan et al., 1990; Shu et al., 2003). Voltages were corrected for the calculated junction potentials (~10 and ~20 mV for current-clamp and voltage-clamp recordings, respectively). The electrical signal for whole-cell recordings (both current-clamp and voltage-clamp configurations) was low-pass filtered at 10 kHz, digitized at 30 kHz, and recorded via either a Digidata 1320 interface (Molecular Devices) or a Spike2 (CED) system.

EPSCs and IPSCs were recorded at −80 and 0 mV, respectively, with >10 Up and Down states recorded at each reversal potential. Series re-

Table 1. Membrane potential dynamics and properties of different excitatory and inhibitory neurons during slow oscillation

	Neural types							
Parameters	A. Pyramidal	B. Stellate	C. FS	D. NPY NGF	E. NPY Non-NGF	F. SOM	G. 5HTR3a	H. VIP
Mean firing rate during Up state (Hz)	4.2 ± 0.4 $^{B–H}$ (0–7; 17)	0.6 ± 0.2 $^{A,C–E,G,H}$ (0–2.5; 16)	9.1 ± 1.9 $^{A,B,D–H}$ (0–45; 32)	0 (23) $^{A–C,F}$	0 (9) $^{A–C,F}$	0.7 ± 0.2 $^{A,C–E,G,H}$ (0–4.2; 34/48)	0 (42) $^{A–C,F}$	0 (19) $^{A–C,F}$
Mean depolarization during Up state (mV)	8.5 ± 0.7 $^{B–H}$ (3.5–15; 17)	2.5 ± 0.3 ^{A,C,D,G,H} (1.1–4.9; 16)	12.3 ± 0.9 $^{A–B,D–H}$ (3.2–25; 32)	6.2 ± 0.3 $^{A–C,E–H}$ (4.1–8.9; 23)	2.6 ± 0.6 ^{A,C,D} (0–4.6; 9)	2.2 ± 0.2 ^{A,C,D,G,H} (0–4.8; 34/48)	1.4 ± 0.2 $^{A–D,F}$ (0–3.6; 42)	1.0 ± 0.3 $^{A–D,F}$ (0–4; 19)
G_e (nS)	0.63 ± 0.06 $^{C,F–H}$ (0.26–0.98; 14)	0.55 ± 0.11 $^{C,F–H}$ (0.2–1.19; 8)	1.35 ± 0.2 ^{A,B,D,F,G} (0.3–2.64; 11)	0.46 ± 0.08 $^{C,F–H}$ (0.3–0.69; 4)	NA	0.14 ± 0.02 $^{A–D}$ (0.1–0.19; 4)	0.15 ± 0.03 $^{A–D}$ (0.07–0.23; 4)	0.11 ± 0.02 $^{A–D}$ (0.06- 0.21; 7)
G_i (nS)	2.24 ± 0.31 $^{C,D,F–H}$ (0.72–4.48; 14)	1.55 ± 0.18 $^{C,D,F–H}$ (0.64–2.29; 8)	0.62 ± 0.12 ^{A,B,F} (0.21–1.66; 11)	0.29 ± 0.07 ^{A,B,F} (0.1–0.39; 4)	NA	0.09 ± 0.005 $^{A–D,G,H}$ (0.08–0.1; 4)	0.56 ± 0.1 ^{A,B,F} (0.29–0.8; 4)	0.35 ± 0.08 ^{A,B,F} (0.18–0.72; 7)
RMP (mV)	−75.4 ± 0.7 $^{B,C,F–H}$ (−82 to −70; 17)	−72.3 ± 0.6 ^{A,C,D} (−78 to −68; 16)	−78.5 ± 0.6 $^{A,B,D–H}$ (−86 to −70; 32)	−75.5 ± 0.8 $^{B,C,F–H}$ (−80 to −62; 23)	−74.1 ± 1.4 ^{C,F} (−82 to −68; 9)	−70.7 ± 0.5 $^{A,C–E}$ (−76 to −66; 32)	−71.7 ± 0.5 ^{A,C,D} (−80 to −63; 42)	−71.4 ± 0.8 ^{A,C,D} (−76 to −63; 19)
Action potential threshold (mV)	−53.8 ± 0.4 $^{C,D,F–H}$ (−56 to −51; 17)	−52.8 ± 0.8 ^{C,D,G,H} (−43 to −58; 16)	−48.1 ± 0.6 $^{A,B,D–F,H}$ (−53 to −43; 32)	−43.5 ± 0.6 $^{A–C,E–G}$ (−49 to −38; 23)	−52.0 ± 1.1 ^{C,D,G,H} (−56 to −46; 9)	−51.4 ± 0.5 ^{A,C,D,G,H} (−56 to −43; 32)	−48.6 ± 0.5 ^{A,B,D,E,F,H} (−54 to −43; 42)	−43.7 ± 0.5 $^{A–C,E–G}$ (−48 to −40; 19)
Input resistance (MΩ)	243 ± 3 $^{B,C,E–H}$ (125–400; 17)	149 ± 16 $^{A,D–H}$ (80–260; 16)	156 ± 8 $^{A,D–H}$ (60–250; 32)	206 ± 11 $^{B,C,E–H}$ (130–340; 23)	385 ± 58 $^{A–D}$ (200–720; 9)	452 ± 28 $^{A–D}$ (190–800; 32)	403 ± 28 $^{A–D,H}$ (200–800; 42)	508 ± 43 $^{A–D,G}$ (250–900; 19)

Values are reported in mean ± SE. Statistical differences between different neurons are reported in superscript alphabet at $p < 0.05$; numbers in parentheses indicate the range and the numbers of recorded neurons, respectively. G_e and G_i, Excitatory and inhibitory conductances, respectively. RMP, Resting membrane potential.

sistance in voltage-clamp recordings was between 8 and 25 MΩ, and was compensated up to 80%. Series resistance was monitored throughout recordings and, if it was >25 MΩ and/or varied >20%, recording was discontinued. Bridge balance and capacitance neutralization were carefully adjusted during whole-cell current-clamp recordings. At the end of the recording session, the electrode was carefully detached from the recorded cell and the slice was kept for another 15–20 min in the recording chamber before being fixed with 4% paraformaldehyde in 0.1 M sodium phosphate buffer (NaPB) for at least 48 h at 4°C. Unless mentioned otherwise, all drugs and chemicals were purchased from Sigma-Aldrich.

Histochemical processing. Histochemical processing for biocytin was performed using procedures similar to those described by Tahvildari and Alonso (2005). Fixed tissue slices were removed from paraformaldehyde solution, washed in 0.1 M NaPB (three times for 5 min each), and processed without further sectioning. Endogenous peroxidase activity was suppressed by incubating slices in 2% H_2O_2 in 0.1 M NaPB for 30 min, followed by washing in 0.1 M NaPB (three times for 5 min each). Nonspecific binding was blocked by incubating the slices in 0.1 M NaPB, 0.5% gelatin, and 0.4% Triton X-100 (PHT) for another 30 min. Then the slices were labeled with an avidin–biotin–horseradish peroxidase complex (Vector Laboratories) in 0.1 M NaPB and 0.4% Triton X-100 overnight. The next day, the slices were washed extensively in PHT: five times for 3 min each, then one time for 30 min, then six times for 1 h each, and finally a wash overnight. The final day, slices were washed with 0.1 M Tris-buffered saline (TBS), pH 7.6 (three times for 10 min each), and then transferred to 3,3-diaminobenzidine solution (DAB substrate solution) (Vector Laboratories). The DAB reaction was stopped when the desired staining intensity was reached by washing the slices in TBS (three times for 10 min each). Finally, the slices were mounted on glass slides, left to air dry for 5 min, and mounted with Mowiol (EMD Serono). The biocytin-filled neurons were reconstructed using the Neurolucida system (MicroBrightField) on a Nikon microscope (Nikon) with a 100× objective.

Data analysis. Electrophysiological data were analyzed using either Clampfit 10 (Molecular Devices) or Spike2 (Cambridge Electronic Design), and graphs were created using Origin 8.0 (OriginLab Corporation). Whole-cell intracellular recordings were segregated into Up/Down states in conjunction with the locally recorded MU network activity. Because our protocols (in current-clamp and voltage-clamp configurations) required moving the membrane potential across a wide voltage range, we used the nearby MU recording as an indicator of the state of the local network. A threshold equal to 1.5 times larger than peak-to-peak baseline noise was set on the MU signals, and a crossing of the threshold, which remained above this threshold for at least 1 s, signified a transition from the Down to the Up state. When the MU signal fell below the threshold, and stayed below threshold for at least 2 s, a transition to the Down state was indicated.

The apparent input resistance was estimated from the voltage deflection after injection of step hyperpolarizing current that changed the membrane potential by ~15 mV from rest. The membrane time constant was taken as the time to reach 63% of steady-state response. Action potential threshold was defined as the V_m when the rate of rise of the spike exceeded 15 V/s. To measure average Up-state excitatory and inhibitory synaptic conductances (G_e and G_i, respectively), first the area under each Up state-associated barrage of EPSCs or IPSCs was measured and the mean amplitude of current calculated. Average Up-state G_e and G_i were computed by recording EPSCs at the experimentally measured reversal potential for inhibition (approximately −80 mV) and by recording IPSCs at the experimentally measured reversal potential for excitation (~0 mV). Values reported in the manuscript, graphs, and Table 1 are mean ± SEM. Statistics were performed with either a *t* test or ANOVA.

Results

The entorhinal cortex robustly generates the slow oscillation *in vitro*

To investigate the distinct roles of different subtypes of cortical interneurons during generation of the slow oscillation *in vitro*, we developed a slice preparation of the mouse EC that generates robust and reliable spontaneous slow neural oscillations in a submersion-style recording chamber. Such a preparation provides the opportunity to take advantage of different transgenic mouse lines expressing EGFP (or hrGFP) in unique interneuronal subpopulations (Oliva et al., 2000; Gong et al., 2003; van den Pol et al., 2009; Taniguchi et al., 2011). Near-horizontal slices of the EC and adjacent cortices of mouse brain (see Materials and Methods) were prepared (Fig. 1*A*). Using four simultaneous extracellular MU glass electrodes locating in different layers (from layers 1 to 6; Fig. 1*B*; $n = 5$), we first observed that perfusing slices with an extracellular solution that contains divalent ion concentrations similar to those found *in vivo* (1 mM Mg^{2+} and 1.2 mM Ca^{2+}) (Zhang et al., 1990), results in spontaneous and robust generation of the slow oscillation (Sanchez-Vives and McCormick, 2000), which was stable for the lifetime (6–8 h) of the EC slices. The generation of this slow oscillation was dependent upon both the upper and lower surface of the slice being exposed to a high flow rate (3–5 ml/min) of well oxygenated extracellular solution, presumably because of the ability of this configuration to deliver oxygen to the tissue (Hájos et al., 2009).

The slow oscillation alternated between Up and Down states (Fig. 1*C*). The Up states are characterized by a robust increase in neuronal activity, as revealed by MU recordings. In the EC, these Up states were markedly long in duration (3.1 ± 0.2 s). Down states are characterized by a relative quiescence of neuronal activity in between adjacent Up states, although on occasion a low level of spontaneous action potential (and synaptic potential) activity was observed. In our slice preparation, the Down states exhibit an average duration of 7.6 ± 0.6 s ($n = 5$; Fig. 1*C*).

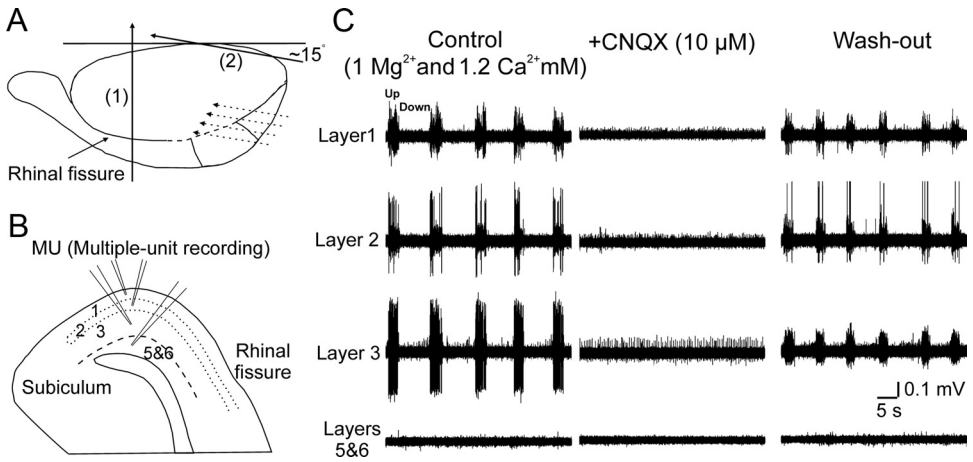

Figure 1. Slices of EC robustly generate the slow oscillation *in vitro*. ***A***, Schematic representation of the semihorizontal angle used to make slices of the entorhinal cortex and adjacent cortical areas. The brain was cut at ~15° angle (cut 2) with respect to the horizontal plane after removing the cerebellum, brainstem, and the rostral portion (cut 1) of the brain. ***B***, Schematic showing locations of an array of four extracellular MU recordings. ***C***, Left column, Recordings from superficial and deep layers reveals the slow oscillation to occur only in layers 1–3 of the entorhinal cortex *in vitro*. No slow rhythm was seen in the deeper layers (5 and 6; $n = 5$). In control condition, the concentration of Mg^{2+} and Ca^{2+} were 1 and 1.2 mM, respectively. Middle column, The slow oscillation was abolished by bath application of the AMPA/kainate receptor antagonist CNQX (10 μM; $n = 5$). Right column, The slow oscillation was retrieved upon washing out CNQX.

The Up states were robustly generated simultaneously in layers 1–3, superficial to the lamina dissecans. The alternation between Up and Down states was very regular. Indeed, the coefficient of variation of the inter-Up state interval during prolonged recordings (>45 min) was only 0.1 ± 0.05 ($n = 5$) (data not shown). Interestingly, and in contrast to slice preparations of ferret visual and prefrontal cortex (Sanchez-Vives and McCormick, 2000; Shu et al., 2003), we did not observe slow oscillation in layers 5 and 6 in the EC slice *in vitro* (Fig. 1*C*) (Cunningham et al., 2006), even though these layers did become strongly active upon the removal of Mg^{2+} from the bath medium, resulting in the generation of epileptiform activity ($n = 3$) (data not shown) (Jones and Heinemann, 1988). This lack of the slow oscillation in layer 5/6 in our preparation most likely results from the relative independence of supragranular and infragranular layers in the entorhinal cortex, since these layers communicate to one another largely through their interactions with the hippocampus (Witter et al., 1989; Lopes da Silva et al., 1990).

The slow oscillation in layers 1–3 was abolished, in a reversible manner, by bath application of the mixed AMPA/kainate receptor antagonist CNQX (10 μM; $n = 3$; Fig. 1*C*). These results indicate that recurrent excitation is crucial for generation of the spontaneous slow oscillation in EC. The superficial layers of the entorhinal cortex contain two major different cell types that may give rise to this recurrent excitation: pyramidal and stellate neurons (Witter et al., 1989; Canto et al., 2008). We next performed whole-cell recordings from these two cell types to determine their action potential and synaptic activity during the generation of this synchronized network oscillation *in vitro*.

Pyramidal and stellate neurons receive a mixture of excitatory and inhibitory synaptic potentials and generate action potentials during Up states

To investigate the membrane potential dynamics of principal excitatory neurons during the slow oscillation *in vitro*, pyramidal ($n = 17$) and stellate ($n = 16$) neurons were recorded in whole-cell current-clamp configuration in layers 2 and 3, positively identified through biocytin labeling and examination of their dendritic/axonal morphology (Klink and Alonso, 1997). Simultaneous whole-cell recordings of pyramidal neurons (layers 2 and 3) and nearby extracellular MU recordings (interelectrode distances, 50–200 μm) revealed that membrane potentials of pyramidal neurons alternate between two distinct states, in tight synchrony with changes in nearby multiple-unit activity (Fig. 2*A*). During the Up state, pyramidal neurons were strongly depolarized by an average of 8.5 mV (±0.7 mV; $n = 17$; Fig. 2*A1*,*C1*, Table 1). Plotting the distribution of membrane potential (following the filtering of action potentials) during the slow oscillation revealed a marked bimodal distribution (Fig. 2*A1*, inset). The depolarization of the Up state resulted in the irregular generation of action potential activity at an average frequency of 4.2 Hz (±0.4 Hz; Fig. 2*C2*, Table 1; including one silent pyramidal cell). Following the cessation of the Up state, these pyramidal cells typically exhibited a prolonged (5–9 s) slow afterhyperpolarization (Fig. 2*A1*). Hyperpolarizing the pyramidal cells by 5–15 mV, such that they were just subthreshold for the generation of action potentials during the slow oscillation, revealed the arrival of synaptic barrages in close relation to the increases in MU activity in the local network with each Up state (Fig. 2*A2*). These synaptic barrages typically were largest at the beginning of the Up state, falling to a less depolarized level just before transition to the Down state (Fig. 2*A2*). During the Down state, synaptic activity returned to a low level of spontaneous events (Fig. 2*A*). Hyperpolarizing single pyramidal neurons by 5–15 mV did not change the rate of occurrence of Up states (0.1 ± 0.01 Hz during control; 0.1 ± 0.009 Hz during hyperpolarization), indicating that they are not generated through ionic mechanisms intrinsic to the recorded neuron. This level of hyperpolarization also did not have strong effects on the amplitude of the synaptic barrages arriving during each Up state in pyramidal neurons (Fig. 2*A*). The abolition of action potential generation during the Up state with hyperpolarization resulted in a large reduction (by 80 ± 2%; $n = 12$) in the afterhyperpolarization occurring during Down states. Since this reduction is much larger than expected for changes in the K^+ driving force alone, we suggest that the spiking activity is responsible for activation of a slow K^+ current, which causes the afterhyperpolarization (Schwindt et al., 1988; Sanchez-Vives and McCormick, 2000; Compte et al., 2003).

Whole-cell recordings from layer 2 stellate neurons revealed this cell type to be less strongly depolarized than neighboring

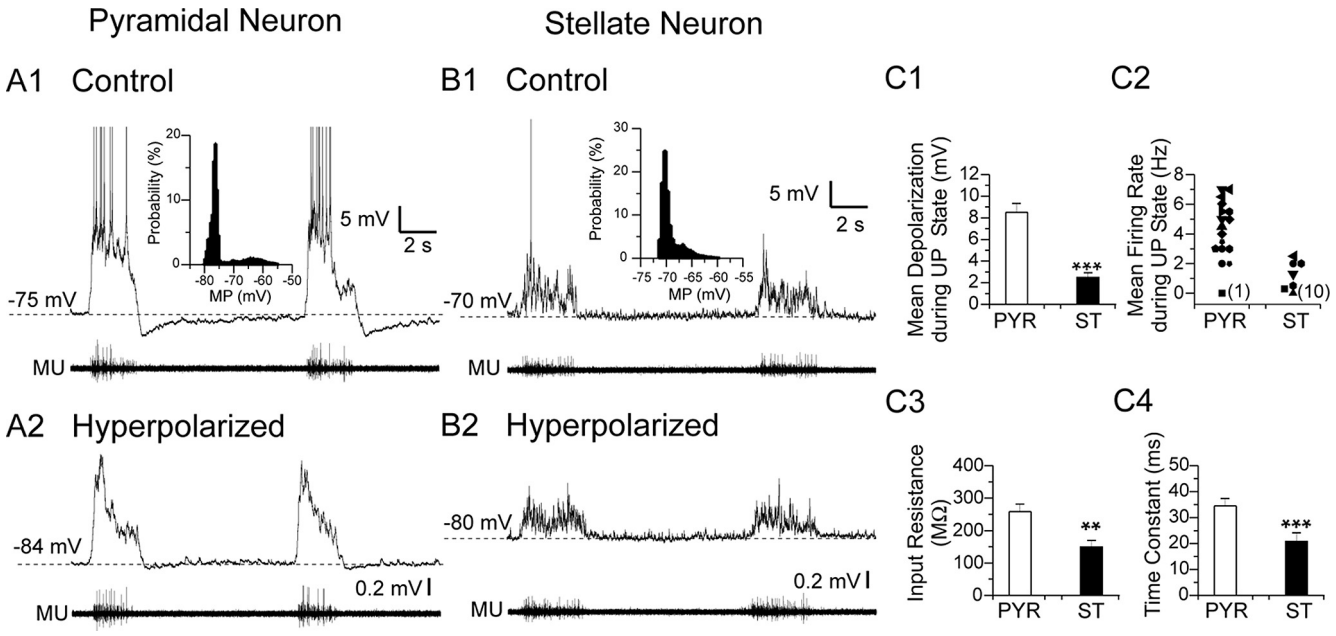

Figure 2. Spontaneous recurrent neural network activity in principal excitatory neurons of the entorhinal cortex *in vitro*. ***A1***, Simultaneous whole-cell (top trace) recording of a layer 3 pyramidal neuron and nearby extracellular MU activity. Inset, The probability histogram of membrane potential values of the neuron in ***A1*** for an epoch of >2 min. The dashed line indicates membrane potential baseline. Action potentials are truncated. Hyperpolarization of the neuron in ***A1*** with intracellular injection of DC reveals the synaptic barrages underlying the depolarizing envelope of the Up state (top trace) that occur simultaneously with local network activity (MU; bottom trace). ***B1***, ***B2***, The same as ***A1*** and ***A2*** except for a layer 2 stellate neuron. Note histogram of distribution of membrane potential in the stellate neuron does not show as strong of a bimodal distribution as observed in pyramidal cells. ***C1–C4***, Bar graphs comparing Up states properties between pyramidal (PYR) ($n = 17$) and stellate (ST) ($n = 16$) neurons. ***C1***, Mean amplitude of depolarization during the Up state. ***C2***, Mean firing rate during Up state. Each symbol represents one recorded neuron except the 10 silent stellate neurons are shown by one symbol. ***C3***, Input resistance. ***C4***, Membrane time constant. $^{**}p < 0.01$, $^{***}p < 0.001$, Student's *t* test. Error bars represent SEM.

pyramidal cells during each Up state (mean amplitude of the Up state from resting membrane potential was 2.5 ± 0.3 mV; Fig. 2*B1*,*C1*, Table 1; *t* test, $p < 0.001$). Plotting the distribution of membrane potentials during the slow oscillation also revealed a distribution that was only weakly bimodal (Fig. 2*B1*, inset). In keeping with this reduced depolarization, most recorded stellate neurons (10 of 16) did not generate action potentials during the Up states, and the average firing rate of the active cells (6 of 16) was only 1.6 Hz (±0.4 Hz; Fig. 2*C2*). Hyperpolarization of stellate neurons by 5–15 mV revealed synaptic barrages arriving in synchrony with extracellular MU activity, as was shown for pyramidal cells. Examining the intrinsic membrane properties of stellate and pyramidal neurons suggested factors contributing to differences between these two cell types. Pyramidal neurons have an average apparent input resistance 243 ± 30 MΩ that is significantly ($p < 0.01$) higher than for stellate neurons (149 ± 16 MΩ; Fig. 2*C3*, Table 1). Similarly, pyramidal neurons, on average, have a membrane time constant (34.5 ± 2.2 ms) that is significantly ($p < 0.001$) longer than observed in stellate neurons (20.8 ± 2.8 ms; Fig. 2*C4*). The larger input resistance and longer time constant of pyramidal neurons, compared with stellate cells, would be expected to allow the same level of excitatory synaptic barrages to depolarize pyramidal cells closer to spike threshold because of enhanced spatiotemporal summation.

To examine the precise nature of the excitatory (EPSC) and inhibitory (IPSC) synaptic currents arriving in principal neurons during Up states, we performed whole-cell recordings in voltage-clamp configuration. To minimize the effect of intrinsic voltage-dependent Na^+ and K^+ currents on synaptically mediated currents, we included QX-314-Cl and Cs^+ in the recording micropipettes (see Materials and Methods). Excitatory synaptic currents were recorded under voltage-clamp mode while holding the cell at approximately −80 mV, which is the experimentally measured reversal of local electrical stimulation evoked $GABA_A$ receptor-mediated IPSCs in pyramidal cells in our preparation (data not shown). Inhibitory synaptic currents were recorded at ~0 mV, which is the experimentally measured reversal potential of EPSCs in pyramidal cells in our preparation (data not shown).

Voltage-clamp recordings revealed that both pyramidal and stellate neurons received a mixture of excitatory and inhibitory currents during Up states (Fig. 3*A*,*B*) and that both cell types receive significantly greater inhibitory, than excitatory, synaptic conductance (Table 1; as observed with our somatic recordings). Plotting the average inhibitory conductance (assuming a reversal potential of −80 mV) versus the average excitatory conductance (0 mV reversal potential) revealed a ratio of 3.56 ± 0.39 for pyramidal cells ($n = 14$) and 3.64 ± 0.76 for stellate neurons ($n = 8$) (Fig. 3*C*). The average excitatory conductance in pyramidal neurons during an Up state (0.63 ± 0.06 nS; $n = 14$) or inhibitory conductance (2.24 ± 0.31; $n = 14$) were not significantly different from those observed in spiny stellate neurons (0.55 ± 0.11 and 1.55 ± 0.18; $n = 8$; respectively; Table 1). As observed previously in ferret cortical pyramidal cells (Shu et al., 2003; Haider et al., 2006), the average excitatory and inhibitory conductances increased and decreased in parallel (data not shown), and yielded an average reversal potential of the Up state-associated synaptic barrages of approximately −55 to −62 mV ($n = 7$). It should be noted that the average conductance during the Up state is significantly smaller than the peak conductance (Figs. 3, 5). While the average reversal potential was typically below firing threshold (approximately −50 to −55 mV) in principal neurons, the variance of the membrane potential allowed brief excursions to above firing threshold, initiating spiking (Fig. 2*A1*,*B1*). Together, we observed that, during the Up state component of the slow oscillation, principal neurons receive a mixture of EPSP(C) and IPSP(C) barrages that significantly depolarizes their membrane

potentials and, in a majority (~65%; 22 of 33 recorded principal neurons) of excitatory cells, results in the generation of action potentials.

While the discharge of pyramidal, and some stellate, neurons is the likely source of the EPSCs arriving in these cells during each Up state, the source of the strong inhibitory synaptic barrages is unknown. To address this question, we performed whole-cell recordings from different subpopulations of interneurons expressing EGFP (or hrGFP) using five different transgenic mouse lines (see Materials and Methods).

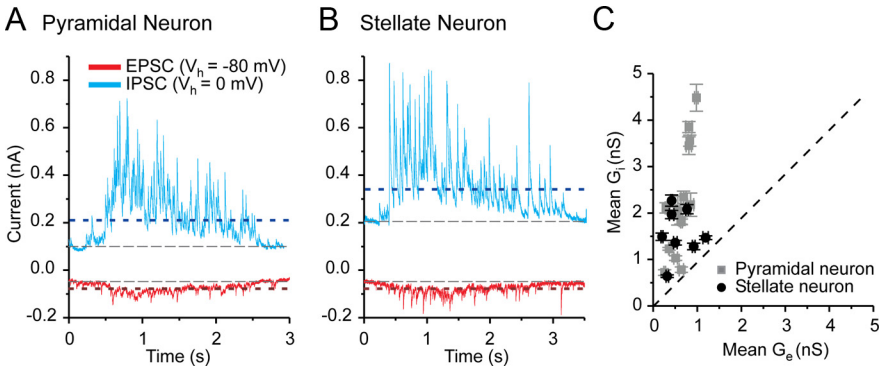

Figure 3. Principal neurons of layers 2/3 of the entorhinal cortex receive strong inhibitory postsynaptic currents during Up states. ***A***, ***B***, Representative current traces during Up state at reversal potentials of excitatory ($V_h \sim 0$ mV; blue traces) and inhibitory ($V_h \sim -80$ mV; red traces) postsynaptic potentials of pyramidal and stellate neurons, respectively. The gray dashed lines indicate baseline; the red and blue dashed lines indicate the mean amplitude of excitatory and inhibitory currents, respectively. ***C***, Scatter plot of the mean inhibitory (G_i) versus mean excitatory (G_e) conductances arriving during an Up state for a population of pyramidal (square symbol; $n = 14$) and stellate (circle symbol; $n = 8$) neurons. Error bars represents SEM.

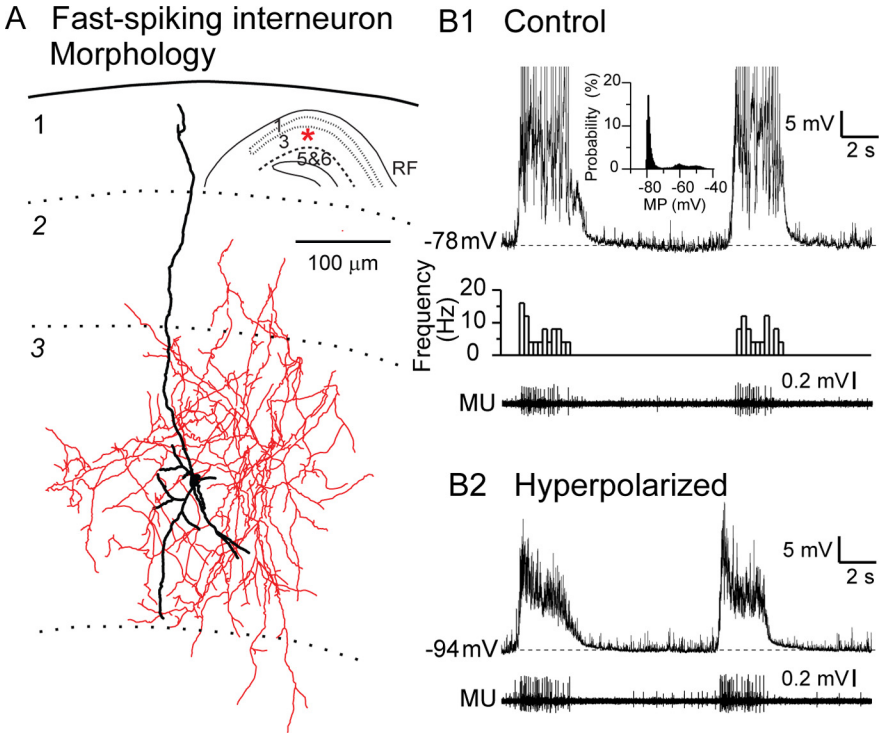

Figure 4. Fast-spiking interneurons are strongly activated during Up states. ***A***, Computer-aided reconstruction of a representative fast-spiking (RCan2-EGFP) interneuron. Soma and dendrites are in black; axon and collaterals are in red. The inset shows the location of the same neuron in the slice. Borders of cortical layers are shown by dotted lines. RF, Rhinal fissure. This neuron had the morphology typical of a basket cell. ***B1***, Membrane potential of a fast-spiking interneuron (top trace), peristimulus histogram (middle panel), and simultaneous MU recordings reveal robust membrane depolarization and action potential generation in FS cells during each Up state. Action potentials are truncated. Inset, The membrane potentials values distribution histogram exhibits a bimodal distribution in this neuron, which was typical of FS interneurons. The dashed lines indicate baseline membrane potential. ***B2***, Hyperpolarization of the same neuron in ***B1*** with DC reveals synaptic barrages during the Up state.

Fast spiking interneurons are strongly excited during Up states

FS cells constitute a major (~30–40%) subtype of GABAergic inhibitory interneuron in layers 2 and 3 of the cerebral cortex (Gonchar et al., 2007), and also in the EC (Miettinen et al., 1996). To target this cell type for whole-cell recordings, we used a mouse line that expresses the fluorescent marker EGFP under the control of the RCan2 promoter (Siddiq et al., 2001). Our whole-cell recordings revealed that all ($n = 32$) EGFP$^+$ cells in the EC of these animals showed electrophysiological properties typical for fast-spiking interneurons. These properties include the ability to generate high-frequency (>200 Hz) trains of relatively thin (duration at half-width, 0.49 ± 0.03 ms; $n = 32$) action potentials in response to a depolarizing current pulses (500 ms; >800 pA) with relatively little or no spike frequency adaptation (McCormick et al., 1985). Reconstruction of the morphological features of these cells revealed that most ($n = 27$ of 32; >80%) possessed the characteristics of basket GABAergic interneurons (Fig. 4*A*) (Marin-Padilla, 1969; Jones and Bühl, 1993). The somato-dendritic morphology of these interneurons was multipolar, with three to six primary aspiny dendrites emanating from the soma. The dense axonal arbors were largely restricted to the same layer in which the soma was located (Fig. 4*A*).

As with pyramidal cells, the membrane potential of FS interneurons was strongly modulated by Up and Down states (Fig. 4*B*) and exhibited a strong bimodality (Fig. 4*B1*, inset). During each Up state, the presence and timing of which was indicated by the nearby extracellular MU recordings, FS (RCan2) interneurons received strong barrages of synaptic potentials, resulting in an average depolarization of 12.3 mV (±0.9 mV; $n = 32$; Table 1). The Up state was associated with a striking increase in FS action potential discharge in the large majority of cells (26 of 32), with the average Up state firing rate being 9.1 Hz (±1.9 Hz; Table 1; including silent neurons). We did not observe any FS interneurons to generate action potentials during the Down state. Hyperpolarizing FS interneurons by 10–20 mV with intracellular injection of current revealed the structure of synaptic barrages during each Up state. As with pyramidal neurons, this hyperpolarization did not alter the frequency of recurrence of the slow oscillation, but did reveal a strong membrane potential bimodality, because of the arrival and withdrawal of synaptic barrages (Fig. 4*B2*).

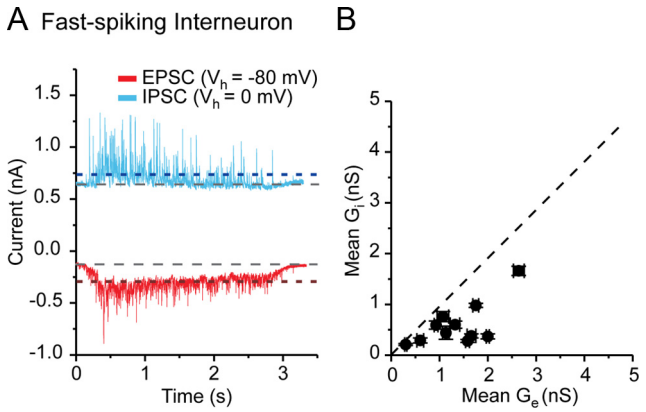

Figure 5. Fast-spiking interneurons receive more excitatory than inhibitory postsynaptic currents during Up states. ***A***, Representative of current traces during Up state at reversal potentials of excitatory ($V_h \sim 0$ mV; blue trace) and inhibitory ($V_h \sim -80$ mV; red traces) currents of a fast-spiking (RCan2-EGFP $^+$) interneuron. The gray dashed lines indicate baseline; the red and blue dashed lines indicate the mean amplitude of excitatory and inhibitory currents, respectively. ***B***, Scatter plot of the mean inhibitory (G_i) versus mean excitatory (G_e) conductances for a population of FS neurons ($n = 11$). Error bars, which are within the size of each data point, represent SEM.

To further investigate the contribution of EPSCs and IPSCs arriving in FS interneurons during the Up state, whole-cell recordings in voltage-clamp mode were performed ($n = 11$). As shown in Figure 5*A*, FS cells were voltage clamped at either the reversal potential for inhibition ($V_h \sim -80$ mV), or for excitation ($V_h \sim 0$ mV) to isolate EPSCs and IPSCs, respectively. During Up states, the average amplitude of the EPSC barrage arriving in FS cells was 2.6 ± 0.5 times greater than the average IPSC barrage (Table 1). Similarly, calculating and plotting the mean inhibitory versus excitatory conductance clearly showed a clear dominance of the excitatory conductance during Up states in FS cells (Fig. 5*B*). The greater excitatory versus inhibitory average synaptic conductance arriving in FS interneurons during the Up state resulted in a more depolarized average reversal potential of the Up state (approximately −25 mV; $n = 8$) than found in pyramidal cells (approximately −62 mV; $n = 7$).

SOM interneurons are weakly excited during Up states

We performed whole-cell recordings from SOM-EGFP-positive interneurons ($n = 48$) in layers 2/3 of EC slices obtained using the GIN mouse line (Oliva et al., 2000). The morphological characteristics as well as passive and active electrophysiological properties of these interneurons in the neocortex have been extensively investigated (Halabisky et al., 2006; Xu et al., 2006; McGarry et al., 2010). In our sample, the majority of SOM interneurons (>70%) in the superficial layers exhibited the morphological characteristics of Martinotti neurons (DeFelipe, 2002). Namely, they gave rise to an ascending axon that originated from a primary dendrite, or less often, from the soma, and that collateralized in both layers 2 and/or 3, and extensively in layer 1 (Fig. 6*A*). Our filled SOM-EGFP cells exhibited a multipolar shaped soma with three to five primary dendrites. Dendritic arborizations in these neurons were less numerous than those of the axon. All SOM interneurons exhibited electrophysiological properties typical for the low-threshold adapting regular spiking category (Beierlein et al., 2003).

Whole-cell recordings of SOM interneurons ($n = 48$) revealed two populations: cells that were silent during the Down state ($n = 34$ of 48) and cells that were spontaneously active, even during the Down state ($n = 14$ of 48). These two populations differed in that the interneurons active during the Down state exhibited a more depolarized membrane potential than the ones silent during the Down state. First, we consider the more common ($n = 34$ of 48) group, which was silent during the Down state. These SOM interneurons received relatively small barrages of synaptic potentials during Up states, with an average amplitude of only 2.2 mV (±0.2 mV) (Fig. 6*B1*, Table 1). These synaptic barrages depolarized the membrane potential from an average of −70.7 mV (±0.5 mV) to −68.5 mV (±0.3 mV). The distribution histograms of the membrane potentials values did not show clear bimodality (Fig. 6*B1*, inset). Most of these interneurons ($n = 23$ of 34) did not spike during Up states, and those that were active discharged only sparsely at an average rate of 1.9 Hz (±0.3 Hz; $n = 11$ of 34). Hyperpolarizing these SOM interneurons through the intracellular injection of current verified the relatively small amplitude of the synaptic barrages arriving in these cells during each Up state (Fig. 6*B2*). Similarly, hyperpolarization of the Down-state active SOM interneurons also revealed small barrages of synaptic potentials during the Up state ($n = 14$) (data not shown). Calculating the excitatory and inhibitory synaptic conductances arriving in these interneurons during the Up state revealed an average G_e of only 0.14 nS (±0.02; $n = 4$) and an average G_i of only 0.09 nS (±0.005 nS; $n = 4$; Table 1).

To examine whether the spontaneous discharge of a subpopulation of SOM interneurons, even during the Down state, resulted from the effects of whole-cell recording, we performed cell-attached single-unit recordings from EGFP $^+$ interneurons in GIN mouse entorhinal cortical slices ($n = 15$). These cell-attached recordings confirmed that a subset of SOM interneurons are spontaneously active, even during the Down state (Down state discharge rate, 0.76 ± 0.23 Hz; $n = 8$ of 15). We noticed that the spontaneously active SOM interneurons were located closer to the upper surface of the slice than the SOM interneurons that were silent during the Down states. Indeed, separating SOM neurons monitored in the cell-attached mode into those recorded at depths of less than or greater than 50 μm from the surface of the slice revealed that SOM interneurons near the surface of the slice were much more likely to be spontaneously active during the Down state. Interneurons recorded near the surface exhibited average spike firing rates of 3.9 ± 1.13 and 0.98 ± 0.34 Hz during Up and Down states (Fig. 6*C*). However, SOM interneurons recorded from deeper locations were significantly ($p < 0.01$) less active during the slow oscillation with average spike frequencies of 1.7 ± 0.57 and 0.11 ± 0.06 Hz during Up and Down states (Fig. 6*C*). Although it is not known why superficial SOM interneurons are more active, one possibility is that the high input resistance (453 ± 28 MΩ; $n = 34$) and prolonged time constant (42.9 ± 4.5 ms) of this cell type makes them very susceptible to small leaks because of damage, such as the cutting of dendritic and axonal processes during slice preparation. A recent study indicates that cells near or on the surface of the slice may have an abnormally high level of internal chloride (Dzhala et al., 2012). The differences in excitability of superficial and deeper SOM cells is unlikely to be related to differences in oxygenation, since the oxygen levels within our slice preparation are high (Yu et al., 2012).

We considered whether the lack of significant synaptic inputs to SOM interneurons during the Up state might be the consequence of the slice preparation, which may have artificially isolated these neurons from synaptic inputs. To address this concern, we introduced Mg^{2+}-free solution to induce epileptiform activity in the slice, reasoning that this manipulation will

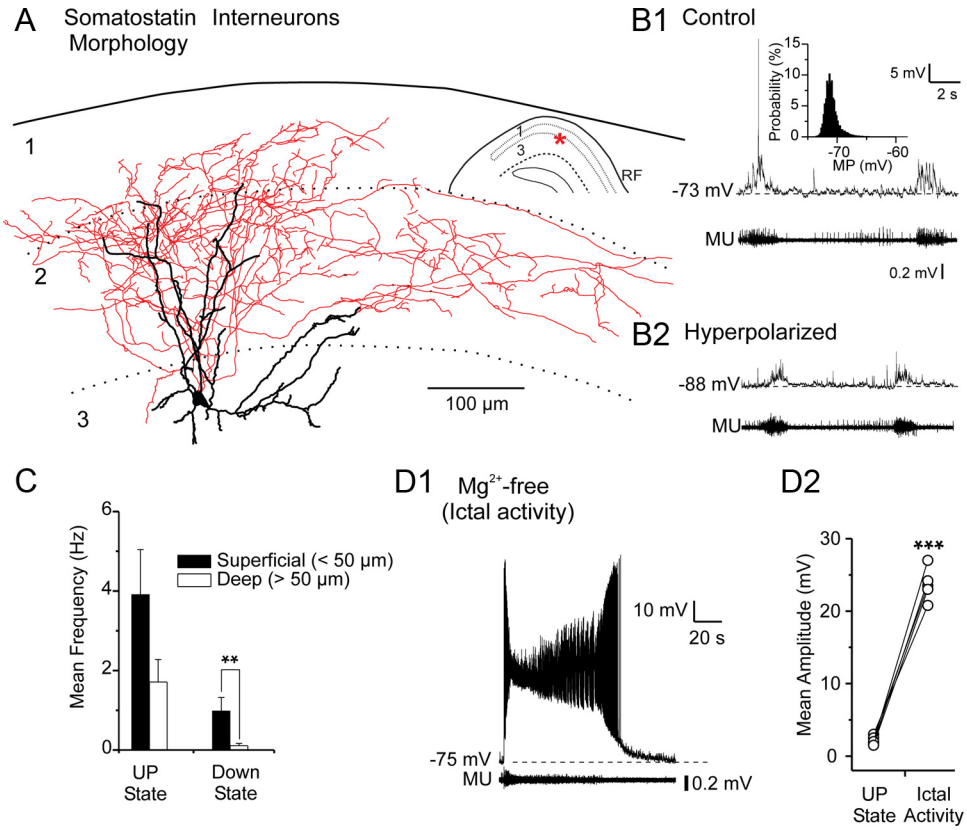

Figure 6. Most somatostatin-positive interneurons are only sparsely active during Up states. ***A***, Computer-aided reconstruction of a representative somatostatin-EGFP interneuron. Soma and dendrites are in black; axons and collaterals are in red. Borders of cortical layers are shown by dotted lines. Action potentials are truncated. The inset shows the location of the same neuron in the slice. RF, Rhinal fissure. ***B1***, Membrane potential of a SOM interneuron (top trace) and simultaneous MU activity recording. During the Up state, the SOM interneuron is lightly depolarized and generates only very sparse (<0.5 Hz) action potential activity. Inset, The membrane potentials values distribution histogram does not show bimodality in this neuron, which is representative of recorded SOM interneurons. ***B2***, Hyperpolarization of the same neuron in ***B1*** with DC (top trace) and simultaneously recorded MU activity (bottom trace). ***C***, Bar graph of the mean frequency of spiking between Up and Down states (in cell-attached mode) of SOM interneurons recorded at two different depths from the upper surface of the slice (**$p < 0.01$, Student's *t* test). ***D1***, Removal of extracellular Mg^{2+} causes spontaneous epileptiform activity. ***D2***, Scatter plot showing the values of mean amplitude deflection of membrane potentials during the normal Up state and following introduction of Mg^{2+}-free solution and the subsequent generation of epileptiform activity. Each symbol represents one cell. ***$p < 0.001$, Student's *t* test. Error bars represent SEM.

strongly activate all excitatory neurons within the tissue (Jones and Heinemann, 1988). Indeed, reducing the bath concentration of Mg^{2+} from 1 mM to nominally Mg^{2+} free abruptly resulted in the appearance 20–45 s periods of strong synchronized bursts of action potential activity (Fig. 6*D1*). Whole-cell recordings from SOM interneurons ($n = 5$) during this rapid transition revealed a shift from the small (<3 mV) synaptic barrages associated with each Up state to very large and prolonged depolarization (peak, >40 mV) during each epileptiform event (Fig. 6*D1*). In this particular condition, SOM interneurons discharged strongly (action potential discharge of 35.8 ± 3.9 Hz) during the epileptiform activity (Fig. 6*D1*; same neuron as *B1*). The average membrane potential deflection during Mg^{2+}-free-induced epileptiform activities was 23.7 mV (±1.1 mV). This result indicates that our slice preparation retains sufficient synaptic connectivity to strongly activate layer 2/3 SOM interneurons.

NPY interneurons possess two distinct groups and do not spike during Up states

We recorded 32 NPY-hrGFP interneurons (van den Pol et al., 2009) in layers 2 and 3 during the slow oscillation *in vitro*. Based on morphological characteristics, intrinsic electrophysiological properties and the amplitude of synaptic barrages that these neurons receive during Up states, we could distinguish two distinct subpopulations of NPY interneuron. The most abundant group exhibited morphological features typical of neurogliaform interneurons (NGF) (Fig. 7*A1*; $n = 23$ of 32) (DeFelipe, 2002; Tricoire et al., 2010). The somata of NGF-NPY interneurons were round and gave rise to between four and nine primary dendrites. The dendrites of NGF-NPY interneurons were beaded and largely restricted to the same layer as the soma, although they occasionally crossed into other layers. The remaining NPY interneurons exhibited non-NGF morphology ($n = 9$ of 32). These non-NGF-NPY interneurons possessed somata that were polygonal in shape giving rise to three to four primary dendrites that spanned several different layers (Fig. 7*B1*). In NGF-NPY interneurons, the axon collateralized extensively and issued a dense intertwined network of collaterals, typically within the same lamina as the cell body. The horizontal extent of these axonal arbors was considerably greater than that of the dendrites (Fig. 7*A1*). In contrast to NGF-NPY interneurons, the non-NGF-NPY interneurons exhibited a significantly less dense and less branched local axonal arbor, although this axonal projection typically spanned several layers (Fig. 7*B1*).

In addition to morphological differences, the two classes of NPY interneurons also could be distinguished based upon their electrophysiological properties. In brief, NGF-NPY interneurons responded to the injection of just suprathreshold depolarization current pulse with a delayed regular spiking pattern (Fig. 7*C1*), as it has been previously reported in rat prefrontal cortex (Kawagu-

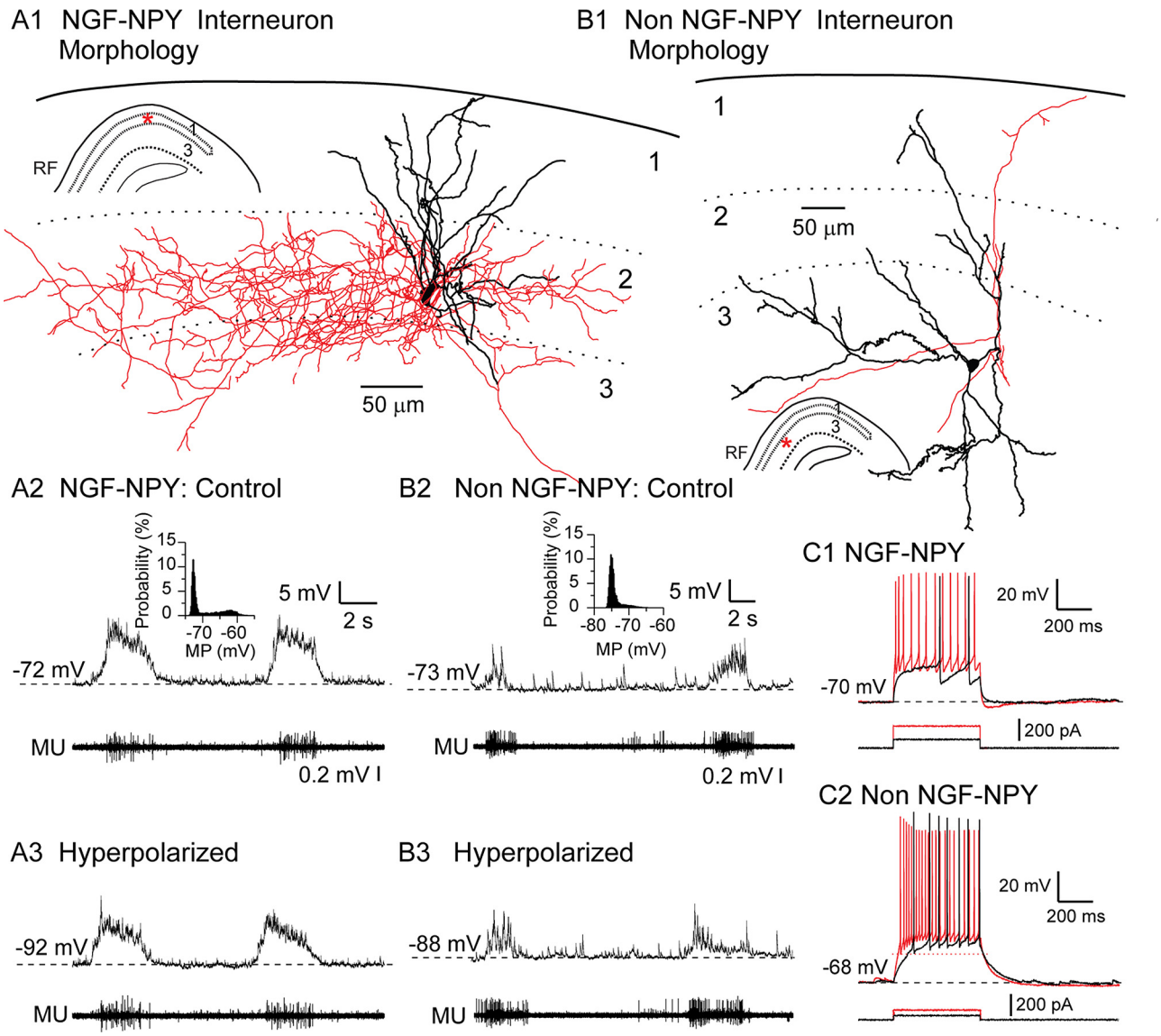

Figure 7. NPY interneurons are not activated during the Up state. ***A1***, Computer-aided reconstruction of a representative NGF NPY interneuron. Soma and dendrites are in black; axon and collaterals are in red. The inset illustrates the location of the same neuron in the slice. RF, Rhinal fissure. ***A2***, Membrane potential of a NGF NPY interneuron (top trace) and simultaneous MU activity reveal significant membrane depolarization, but the absence of action potentials, during each Up state. Inset, The membrane potentials values distribution histogram shows a bimodal distribution, which was typical of NGF NPY interneurons. ***A3***, Hyperpolarization of the same neuron in ***A2*** with DC (top trace) and simultaneous MU activity (bottom trace). ***B1***, Computer-aided reconstruction of a representative of non-NGF NPY interneuron. Soma and dendrites are in black; axon and collaterals are in red. The inset illustrates the location of the same neuron in the slice. RF, Rhinal fissure. ***B2***, ***B3***, Same as ***A1*** and ***A2*** for a non-NGF NPY interneuron. ***C1***, ***C2***, Representative voltage responses to step depolarizing-current pulses in NGF and non-NFG NPY interneurons. Note the delayed spiking to just subthreshold current pulse in the NGF neurons, and also the low threshold spiking property in non-NGF neurons.

chi and Kubota, 1997). However, injection of depolarizing current pulses into non-NGF NPY interneurons resulted in a low-threshold adapting regular spiking action potential response (Fig. 7*C2*) (Beierlein et al., 2003).

Neurogliaform-NPY interneurons received strong synaptic barrages during each Up state, resulting in a significant depolarization that averaged 6.2 mV (±0.3 mV; $n = 23$; Table 1, Fig. 7*A2*). Because of the substantial depolarization during the Up state, plotting the distribution of membrane potential in these cells during the slow oscillation revealed significant bimodality (Fig. 7*A2*, inset). The synaptic barrages arriving in NGF-NPY neurons exhibited a reduced level of higher frequency membrane potential fluctuations, compared with pyramidal and stellate neurons or FS interneurons (compare Figs. 2, 4). Interestingly, despite the significant membrane depolarization associated with each Up state during the slow oscillation *in vitro*, the NGF-NPY interneurons did not generate action potentials. The synaptic barrages never reached action potential threshold, which is significantly depolarized in these cells compared with other cell types (action potential threshold, −43.5 ± 0.6; $n = 23$; Table 1). The Up state depolarization in NGF-NPY neurons resulted from a significant increase in average excitatory synaptic conductance (0.48 nS; Table 1), which was greater than the average inhibitory synaptic conductance (0.29 nS; $n = 4$), yielding a calculated reversal potential for the synaptic barrages of −28 mV (data not shown).

In contrast to NGF-NPY cells, non-NGF-NPY interneurons received significantly less depolarizing synaptic barrages during Up states, averaging only 2.6 mV (±0.6 mV; $n = 9$; Fig. 7*B2*, Table 1) in amplitude. The non-NGF-NPY interneurons, as the

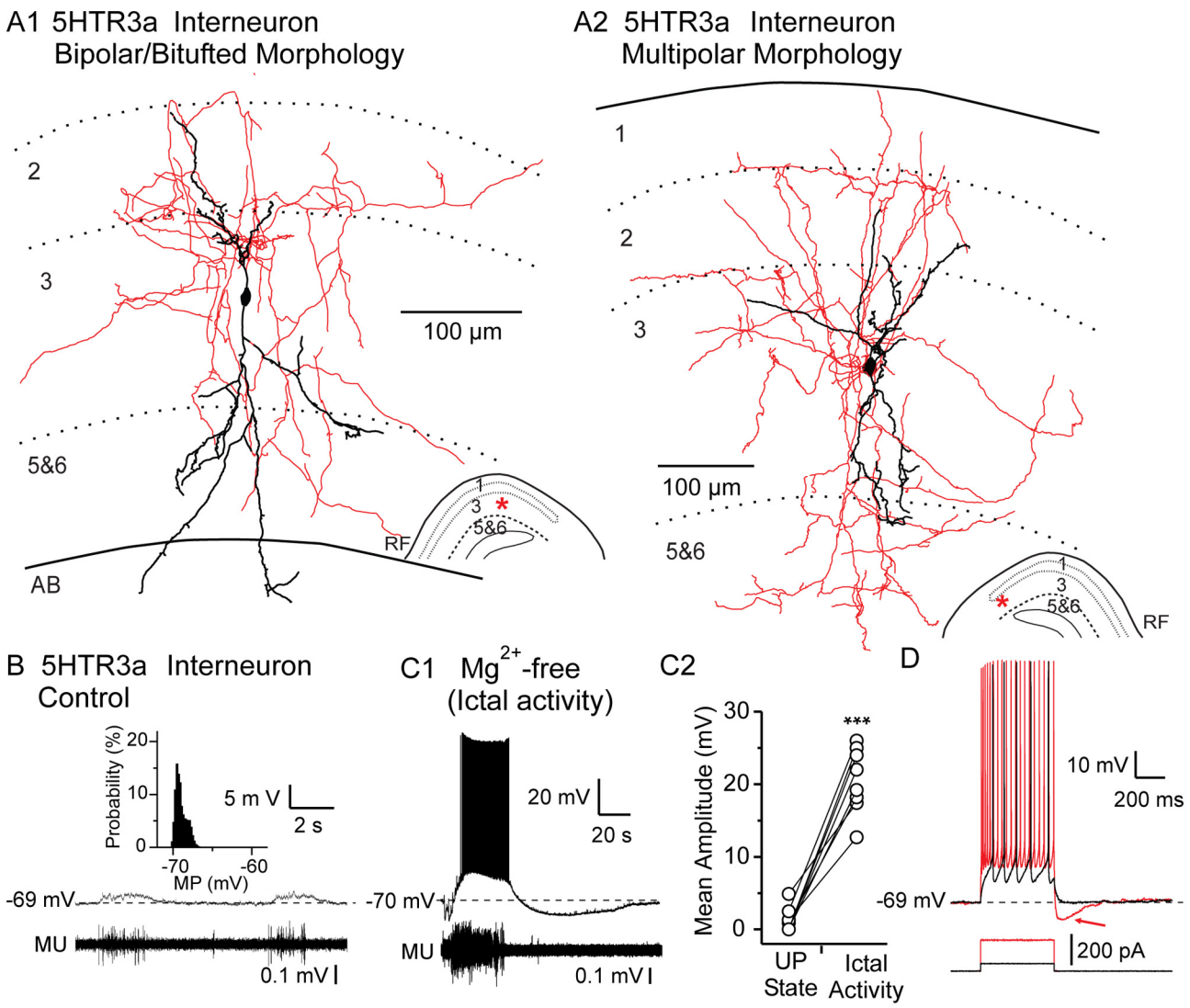

Figure 8. Interneurons expressing ionotropic serotonin receptors (5HTR3a) receive a negligible amount of synaptic barrages during each Up state. ***A1***, ***A2***, Computer-aided reconstruction of 5HTR3a interneurons with bipolar and multipolar morphology, respectively. Soma and dendrites are in black; axon and collaterals are in red. The insets illustrate locations of the corresponding neurons in the slice. The dotted lines indicate the boarders between different layers. RF, Rhinal fissure; AB, angular bundle. ***B***, Membrane potential of a 5HTR3a interneuron (top trace) and simultaneous MU activity recordings indicate only slight (~2 mV) membrane depolarization and the absence of action potential generation during each Up state. The trace belongs to a bipolar interneuron. ***C1***, Removal of extracellular Mg^{2+} causes spontaneous epileptiform activity. Simultaneous intracellular recording of membrane potential (top trace) of the same 5HTR3a interneuron shown in ***A*** and MU activity (bottom trace). ***C2***, Scatter plot showing the average membrane potential deflection during the Up state and following removal of Mg^{2+} from the bath solution. Each symbol represents one cell. ***$p < 0.001$, Student's t test. ***D***, Membrane potential voltage responses to two depolarizing current pulses in a representative of 5HTR3a interneuron. Note the significant AHP (red arrow) following repetitive firing, which is characteristic of 5HTR3a interneurons.

NGF-NPY interneurons, did not spike during Up states. Perhaps because of a less intense synaptic barrage during each Up state, the synaptic potentials arriving in non-NGF NPY neurons were individually more distinct than those in NGF-NPY neurons (Fig. 7*A2*,*B2*). The average amplitude of synaptic conductances arriving in this cell type was not determined. Examining the apparent input resistance of the two subtypes of NPY interneurons revealed a significantly lower value for the NGF versus the non-NGF NPY interneurons (206 ± 11 and 385 ± 58 MΩ, respectively; t test, $p < 0.001$; Table 1). Thus, differences in apparent input resistance cannot explain the differences in synaptic barrages experienced by the two subtypes of NPY interneuron.

5HTR3a interneurons receive relatively sparse synaptic potentials during Up states

A recent study demonstrated that neurons expressing the ionotropic 5HT3a receptor gene comprise a morphologically/electrophysiologically diverse subgroup of interneurons in the superficial layers of the somatosensory cortex that accounts for a significant fraction of inhibitory interneurons (Lee et al., 2010). Morphologically, 5HTR3a-EGFP interneurons in layers 2 and 3 of the EC fell into two broad groups. The majority of these interneurons (>60%; $n = 28$ of 42) exhibited a bipolar/bitufted morphology with two primary dendrites emanating in opposite directions (Fig. 8*A1*). Somata of these bipolar shape interneurons were spindle or ovoid in shape. The dendritic arborizations of these interneurons could span several cell layers (Fig. 8*A1*). The axonal tree of these bipolar/bitufted interneurons was not as extensive or dense as those observed in other types of interneurons (e.g., RCan2); however, the axons of these cells could extend across laminae into more superficial layers and occasionally to deeper layers (Fig. 8*A1*). The other broad category of 5HTR3a neurons exhibited a multipolar shape ($n = 14$ of 42), with locally ramifying, three to five short dendrites, that remained largely

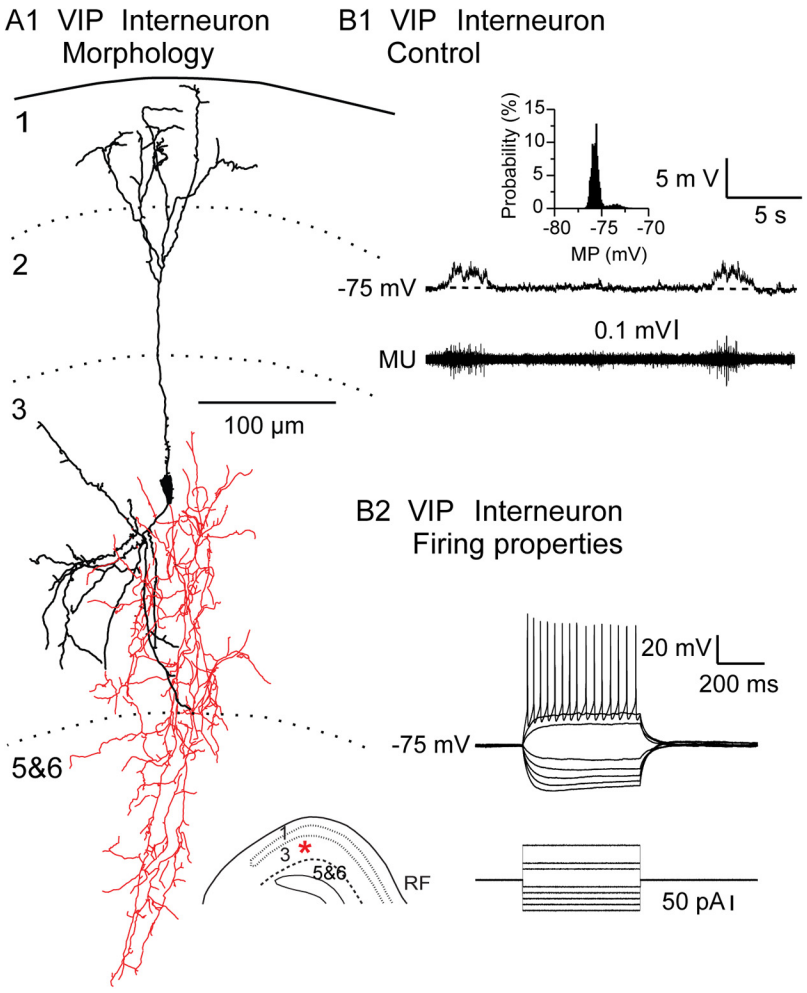

Figure 9. Interneurons expressing VIP receive only a light barrage of synaptic inputs during the Up state. ***A***, Dendritic and axonal morphology of a representative VIP interneuron. Soma and dendrites are in black; axon and collaterals are in red. The inset illustrates location of the same neuron in the slice. RF, Rhinal fissure. ***B1***, Membrane potential of a VIP interneuron (top trace) and simultaneous MU activity recordings indicate small (~1 mV average) membrane depolarization and the absence of action potential generation during each Up state. Inset, Membrane potential probability histogram. ***B2***, Membrane potential responses to a series of hyperpolarizing and depolarizing current steps.

within the same layer as the soma. These cells exhibited a local axonal plexus that was also limited mainly to the same layer as the soma (Fig. 8*A2*). The vast majority ($n = 40$ of 42) of the 5HTR3a interneurons responded to a depolarizing current pulse with an adapting regular spiking pattern of action potential generation that was followed by a marked afterhyperpolarization (Fig. 8*D*). We did not observe any striking difference in the firing properties of the bipolar and multipolar 5HTR3a morphological subtypes.

Simultaneous extracellular and whole-cell recordings revealed that, while the EC slices generated robust Up states, layer 2/3 5HTR3a interneurons received only negligible synaptic barrages (average depolarization of 1.4 ± 0.2 mV; Table 1) and failed to generate action potentials (Fig. 8*B*) despite their high input resistance (Table 1). This small depolarization resulted both from a relatively small average excitatory conductance (0.15 nS; Table 1), and a proportionally large bombardment by inhibitory synaptic potentials (0.53 nS; Table 1).

To ensure that the local network was capable of exciting 5HTR3a neurons, we removed Mg^{2+} from the bathing medium, to induce epileptiform activity (Fig. 8*C1*). Strong bursts of MU activity within the local network during the epileptiform event was associated with the large depolarization (average of 20.6 ± 1.6 mV) of 5HTR3a neurons and the generation of pronounced trains of action potentials (Fig. 8*C1*,*C2*; $n = 8$). These results indicate that EC slice preparation retains sufficient connectivity to robustly activate 5HTR3a interneurons, but fails to do so during normal Up states of the slow oscillation.

VIP interneurons receive sparse synaptic barrages during Up states

We performed whole-cell recordings in current-clamp configuration from 19 neurons expressing Zs-green in VIP-containing interneurons (see Materials and Methods) in layers 2 and 3 of the EC simultaneously with extracellular multiple unit recording during spontaneous neural network activity (Up/Down states). Morphologically, the large majority (16 of 19) of these interneurons appeared as double bouquet cells (Fig. 9*A*). The somata of these cells were spindle or ovoid in shape, with one or two primary apical and basal dendrites emanating from the soma. The dendrites typically reached superficially to layer 1 and the pia, and at least to the upper parts of layers 5/6 (Fig. 9*A*). An axon originated, in most cases, from the basal part of the soma and traveled down toward the deeper layers (5 and 6). Here, the axon branched extensively, exhibiting intertwined basal axon collaterals characteristics of the double bouquet morphology (Kawaguchi and Kubota, 1997). The majority of the VIP interneurons ($n = 14$ of 19) responded to a depolarizing current pulse with an adapting regular spiking pattern of action potential (Fig. 9*B2*), while the remaining neurons ($n = 5$ of 19) generated irregular spiking during application of a step depolarizing current pulse (data not shown).

Simultaneous extracellular and whole-cell recordings revealed that, while there is robust neural network activity in layers 2 and 3 of the EC, adjacent VIP interneurons received only small synaptic barrages (average depolarization of 1.0 ± 0.3 mV; Table 1) and failed to generate action potentials (Fig. 9*B1*). Because of the small average amplitude of synaptic barrages, VIP interneurons do not show a significant bimodality in their membrane potential during Up/Down states (Fig. 9*B1*, inset). Similar to other tested interneurons (e.g., SOM, 5HTR3a), the generation of epileptiform activity through the removal of Mg^{2+} from the bathing medium resulted in intense action potentials discharges in VIP interneurons ($n = 3$) (data not shown). These results indicate that EC slice preparation possesses sufficient connectivity to robustly activate VIP interneurons, but fails to do so during normal Up states of the slow oscillation. Further investigations on the nature of the synaptic conductances that these interneurons receive during the Up state revealed that the small depolarization resulted from a mixture of small excitatory conductance

(0.11 nS; Table 1), and a slightly larger inhibitory synaptic conductance (0.35 nS; Table 1).

Discussion

We have developed an *in vitro* submerged slice preparation of mouse entorhinal cortex that robustly and spontaneously generates the cortical slow oscillation. Our study suggests that the functional interactions between different types of neurons, as revealed by the slow oscillation, vary from cell type to cell type and are highly specific (Fig. 10). By recording the activity of five different subtypes of interneuron, which collectively account for the large majority of GABAergic cells in layers 2/3, and two types of excitatory neurons, we found that inhibitory neurons containing somatostatin, neuropeptide Y, vasoactive intestinal peptide, or the 5HTR3a receptor generate either very few or no action potentials during the Up state *in vitro*, while fast-spiking interneurons and pyramidal neurons are highly active. Our data indicate that the recurrent interactions between excitatory pyramidal neurons and fast-spiking inhibitory interneurons mainly generate the persistent activity of the Up state, which in many ways is similar to the maintained but variable depolarization of the awake, attentive state *in vivo* (Steriade et al., 2001; Destexhe et al., 2007).

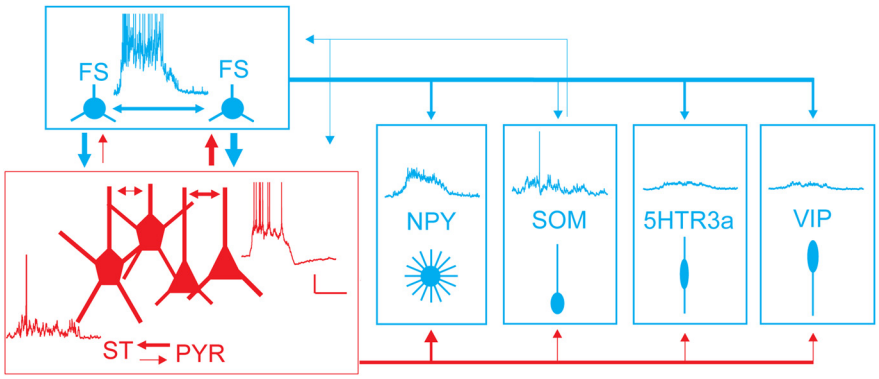

Figure 10. Summary diagram illustrating the proposed interactions between cortical neuronal subtypes, as revealed by the generation of Up states. Note that scale bars for pyramidal (PYR) neurons apply to all other traces. The Up states are generated by a recurrent interaction between PYR neurons and FS interneurons, with less involvement of ST and SOM neurons. The FS interneurons also project to one another, regulating their response to the excitatory potentials initiated by PYR and ST neurons. Nearby NPY interneurons are also depolarized by activity in excitatory and inhibitory FS neurons, but this does not reach action potential threshold. SOM interneurons receive mild excitatory inputs, which occasionally bring the cell to discharge. In contrast, both 5HTR3a and VIP interneurons receive relatively little synaptic input, despite the strong action potential barrages in nearby PYR and FS neurons. The arrows with different thickness indicate the relative strength of the functional connections between pyramidal/stellate neurons, FS interneurons, and the other subtypes of interneurons recorded. These results reveal a remarkable specificity and heterogeneity in the interconnections of pyramidal cells and different subtypes of inhibitory interneurons in the cerebral cortex.

Synaptic barrages to principal neurons and local interneurons during slow oscillation

Previous *in vivo* and *in vitro* studies have demonstrated that excitatory and inhibitory postsynaptic potentials (currents) arriving in pyramidal neurons during spontaneous Up states are highly interrelated, both in their amplitude, which is roughly proportional on average, as well as timing (Shu et al., 2003; Hasenstaub et al., 2005; Haider et al., 2006). In our present recordings, we observed that both pyramidal and stellate neurons were depolarized by barrages of EPSPs during each Up state, although these were intermixed with IPSPs that were on average approximately three times larger in conductance (Table 1), indicating that at least one population of inhibitory interneuron in the cortex is strongly activated by the Up state. The higher firing rate of pyramidal versus stellate neurons during each Up state is likely to have resulted in part from the higher input resistance of the former, which facilitates the ability of the synaptic barrage to depolarize the neuron toward firing threshold (Table 1). Interneurons, like pyramidal and stellate neurons, also received barrages of EPSPs and IPSPs during the Up state in our preparation, although the precise mix of these and their functional effects varied markedly between cell types (Table 1).

Fast-spiking inhibitory interneurons, which typically are basket or chandelier cells (McCormick et al., 1985; Kawaguchi et al., 1987; Kawaguchi and Kubota, 1997), received strong barrages of EPSPs, which were associated with an even larger increase in excitatory conductance than observed in pyramidal and stellate neurons. This potent EPSP barrage was offset by a moderate average amplitude IPSP barrage, resulting in fast-spiking GABAergic neurons being strongly driven to discharge during each Up state. These strong barrages of EPSPs are consistent with the high degree of connectivity between excitatory neurons and FS GABAergic cells (Reyes et al., 1998; Beierlein et al., 2003; Levy and Reyes, 2012). Of the four other subtypes of GABAergic interneurons that we examined, only the NGF-NPY cells received EPSP barrages that were comparable in amplitude to those of excitatory neurons (Table 1). This result indicates that the local connections of layer 2/3 pyramidal cells are highly selective, strongly innervating other pyramidal/stellate neurons as well as FS and NPY GABAergic interneurons, while only sparsely activating other types of local inhibitory cells. Even though the synaptic barrages in NGF-NPY neurons resulted in a significant depolarization of the somatic membrane potential, these cells were never observed to discharge during the Up state, in part because of a high spike threshold (Table 1). The other three interneuron subtypes, SOM, 5HTR3a, and VIP, received only light excitatory synaptic barrages during each Up state. These three cell types, however, differed in an important manner. 5HTR3a and VIP interneurons received an IPSP barrage that was significantly stronger (approximately threefold) than the EPSP barrage. These IPSP barrages in 5HTR3a and VIP interneurons were approximately as strong as that occurring in fast-spiking GABAergic interneurons (Table 1). Since the FS GABAergic cells were the only inhibitory interneuron subgroup to discharge strongly, these data suggest that this cell class projects widely to multiple cell types (pyramidal, stellate, FS, 5HT3a, VIP), with the possible exception of SOM and NPY interneurons (Fig. 10). The mixture of small EPSP amplitude with moderate IPSP amplitude prevented 5HTR3a and VIP cells from generating action potentials during the Up state. In contrast, SOM interneurons were driven to discharge at a low rate because of the relative lack of IPSPs, a high input resistance, and a smaller difference between resting membrane potential and spike threshold than observed in other neurons (Table 1). These results emphasize the importance of multiple factors in determining whether or not a given neuron or neuronal subtype participates in a network activity. These factors include not only anatomical connectivity but also the resting membrane potential, electrotonic structure of the cell (e.g., input resistance, dendritic integration), spike threshold, properties and distribution of ionic

currents, pattern of presynaptic network activity, and synaptic release properties, among other features. The mix of these features results in a highly dynamic network in which individual neurons, or classes of neurons, may be active under only selected conditions (Klausberger et al., 2003).

Firing properties of different types of interneurons during Up state

The unique action potential properties of fast-spiking inhibitory interneurons, which are typically basket and chandelier GABAergic cells (Kawaguchi and Kubota, 1997), have allowed these cells to be monitored during the generation of the recurrent network activity of the Up state *in vitro* (Shu et al., 2003; Cunningham et al., 2006; Fanselow and Connors, 2010) as well as *in vivo*, in the anesthetized (Steriade et al., 1993; Haider et al., 2006), and slow wave sleep state (Steriade et al., 2001). In rodents, slow rhythmic activity remarkably similar to the slow oscillation of sleep and anesthesia is also present in the somatosensory cortex during quiet waking in head-fixed mice (Petersen et al., 2003). In all of these preparations, fast-spiking inhibitory interneurons are highly active, typically the most active neurons recorded, with average discharge rates of ~11 Hz (Haider et al., 2006; Gentet et al., 2010). Given that many fast spiking inhibitory interneurons densely contact neighboring pyramidal and at least some other subtypes of GABAergic interneurons (Galarreta and Hestrin, 1999; Gibson et al., 1999; Thomson and Lamy, 2007; Packer and Yuste, 2011), we can safely assume that a significant portion of the IPSPs arriving in these cells during the Up state arises from the activity of the FS neuronal network (Fig. 10).

The other major category of interneuron that has been studied during cortical network activity are the somatostatin-containing cells, as examined through use of the GIN mouse line (Fanselow and Connors, 2010; Gentet et al., 2012). Excitatory synaptic inputs from single cortical pyramidal cells onto somatostatin containing interneurons exhibit relatively small amplitude (average of ~0.3 mV) and low probability of release (~0.3) (Reyes et al., 1998; Kapfer et al., 2007; Silberberg and Markram, 2007; Fanselow et al., 2008). However, with repetitive activation, these pyramidal cell synapses strongly facilitate and can drive postsynaptic somatostatin interneurons to generate spikes, given a sufficiently intense burst of presynaptic action potentials. In our study, pyramidal cells discharged an average of 14 spikes at ~4 Hz during each Up state. This intensity of discharge is significantly below the number of action potentials and range of frequencies associated with facilitation at pyramidal synapses onto SOM interneurons (Reyes et al., 1998; Kapfer et al., 2007; Fanselow et al., 2008). Thus, during normal Up-state activity, the synapses of pyramidal neurons onto SOM interneurons may remain unfacilitated and small. In contrast, when the tissue generates epileptiform activity because of the removal of Mg^{2+} from the bath (as done in the present study), the intense discharge in nearby pyramidal cells may result in strong depolarization of somatostatin interneurons through multiple mechanisms, including increases both in the number of excitatory neurons discharging and their spatial/temporal summation, and facilitation of their postsynaptic effects.

A recent study (Fanselow and Connors, 2010) has also addressed the role of regular spiking pyramidal neurons and two different types of interneurons (FS and somatostatin interneurons, as recorded in the GIN mouse line) in a cortical slice preparation generating periodic bursts of activity reminiscent of Up states. In contrast to the majority of our recordings, this study observed all SOM interneurons to be active during both Up and Down states. Although not explicitly studied, these interneurons appeared to receive relatively weak barrages of synaptic potentials with each Up state [Fanselow and Connors (2010), their Fig. 1, Table 1], in similarity to our observations. The differences in activity in SOM interneurons between our present study and that of Fanselow and Connors may have resulted from differences in the bath $[Ca^{2+}]_o$ (1.0 mM in the Fanselow and Connors study vs 1.2 mM used in the present study), the depth of the cells recorded (Fig. 6*C*), or other differences in the slice preparations used. A recent *in vivo* study found that SOM interneurons are spontaneously active during quiet wakefulness, perhaps because of their relatively depolarized resting membrane potential (Table 1), but do not receive significant barrages of synaptic potentials during slow-wave oscillations during quiet wakefulness (Gentet et al., 2012).

Recordings from identified inhibitory interneurons *in vivo* indicate that the activities of these cells are state dependent (Gentet et al., 2010, 2012). In the quiet resting mouse, large fluctuation of the membrane potentials, resembling the slow oscillation of sleep, are prevalent in the somatosensory cortex (Petersen et al., 2003). During each depolarized, Up-like state, of these quiet-waking oscillations, fast spiking neurons discharge in a manner similar to that observed here, whereas regular spiking GABAergic interneurons discharge at rate that is less than that of fast spiking interneurons (Gentet et al., 2010). However, when the waking animal actively moves its whiskers, the slow oscillation ceases and the membrane potential loses the prominent Down states. Surprisingly, the average action potential activity of fast-spiking and SOM interneurons decreases, while other types of non-fast-spiking inhibitory interneurons increases (Gentet et al., 2010, 2012). Our findings reveal that, despite the suggestion of panconnectivity of local excitatory-inhibitory interactions (Fino and Yuste, 2011; Packer and Yuste, 2011), the subtypes of inhibitory interneurons in the cortex exhibit a high degree of unique functional interconnectivity (Haider and McCormick, 2009), resulting in the different cell types responding to behavioral demands in specialized ways that depends not only upon the anatomical connections of the circuit but also the state of neuromodulatory networks and the pattern of presynaptic cortical activity (Fig. 10).

References

Ascoli GA, Alonso-Nanclares L, Anderson SA, Barrionuevo G, Benavides-Piccione R, Burkhalter A, Buzsáki G, Cauli B, Defelipe J, Fairén A, Feldmeyer D, Fishell G, Fregnac Y, Freund TF, Gardner D, Gardner EP, Goldberg JH, Helmstaedter M, Hestrin S, Karube F, et al. (2008) Petilla terminology: nomenclature of features of GABAergic interneurons of the cerebral cortex. Nat Rev Neurosci 9:557–568.

Beierlein M, Gibson JR, Connors BW (2003) Two dynamically distinct inhibitory networks in layer 4 of the neocortex. J Neurophysiol 90:2987–3000.

Canto CB, Wouterlood FG, Witter MP (2008) What does the anatomical organization of the entorhinal cortex tell us? Neural Plast 2008:381243.

Compte A, Sanchez-Vives MV, McCormick DA, Wang XJ (2003) Cellular and network mechanisms of slow oscillatory activity (<1 Hz) and wave propagations in a cortical network model. J Neurophysiol 89:2707–2725.

Connors BW, Prince DA (1982) Effects of local anesthetic QX-314 on the membrane properties of hippocampal pyramidal neurons. J Pharmacol Exp Ther 220:476–481.

Cunningham MO, Pervouchine DD, Racca C, Kopell NJ, Davies CH, Jones RS, Traub RD, Whittington MA (2006) Neuronal metabolism governs cortical network response state. Proc Natl Acad Sci U S A 103:5597–5601.

DeFelipe J (2002) Cortical interneurons: from Cajal to 2001. Prog Brain Res 136:215–238.

Destexhe A, Hughes SW, Rudolph M, Crunelli V (2007) Are corticothalamic "up" states fragments of wakefulness? Trends Neurosci 30:334–342.

Dzhala V, Valeeva G, Glykys J, Khazipov R, Staley K (2012) Traumatic al-

terations in GABA signaling disrupt hippocampal network activity in the developing brain. J Neurosci 32:4017–4031.
Fanselow EE, Connors BW (2010) The roles of somatostatin-expressing (GIN) and fast-spiking inhibitory interneurons in UP-DOWN states of mouse neocortex. J Neurophysiol 104:596–606.
Fanselow EE, Richardson KA, Connors BW (2008) Selective, state-dependent activation of somatostatin-expressing inhibitory interneurons in mouse neocortex. J Neurophysiol 100:2640–2652.
Fino E, Yuste R (2011) Dense inhibitory connectivity in neocortex. Neuron 69:1188–1203.
Galarreta M, Hestrin S (1999) A network of fast-spiking cells in the neocortex connected by electrical synapses. Nature 402:72–75.
Gentet LJ, Avermann M, Matyas F, Staiger JF, Petersen CC (2010) Membrane potential dynamics of GABAergic neurons in the barrel cortex of behaving mice. Neuron 65:422–435.
Gentet LJ, Kremer Y, Taniguchi H, Huang ZJ, Staiger JF, Petersen CC (2012) Unique functional properties of somatostatin-expressing GABAergic neurons in mouse barrel cortex. Nat Neurosci 15:607–612.
Gibson JR, Beierlein M, Connors BW (1999) Two networks of electrically coupled inhibitory neurons in neocortex. Nature 402:75–79.
Gonchar Y, Wang Q, Burkhalter A (2007) Multiple distinct subtypes of GABAergic neurons in mouse visual cortex identified by triple immunostaining. Front Neuroanat 1:3.
Gong S, Zheng C, Doughty ML, Losos K, Didkovsky N, Schambra UB, Nowak NJ, Joyner A, Leblanc G, Hatten ME, Heintz N (2003) A gene expression atlas of the central nervous system based on bacterial artificial chromosomes. Nature 425:917–925.
Haider B, McCormick DA (2009) Rapid neocortical dynamics: cellular and network mechanisms. Neuron 62:171–189.
Haider B, Duque A, Hasenstaub AR, McCormick DA (2006) Neocortical network activity *in vivo* is generated through a dynamic balance of excitation and inhibition. J Neurosci 26:4535–4545.
Hájos N, Ellender TJ, Zemankovics R, Mann EO, Exley R, Cragg SJ, Freund TF, Paulsen O (2009) Maintaining network activity in submerged hippocampal slices: importance of oxygen supply. Eur J Neurosci 29:319–327.
Halabisky B, Shen F, Huguenard JR, Prince DA (2006) Electrophysiological classification of somatostatin-positive interneurons in mouse sensorimotor cortex. J Neurophysiol 96:834–845.
Hasenstaub A, Shu Y, Haider B, Kraushaar U, Duque A, McCormick DA (2005) Inhibitory postsynaptic potentials carry synchronized frequency information in active cortical networks. Neuron 47:423–435.
Jones RS, Bühl EH (1993) Basket-like interneurones in layer II of the entorhinal cortex exhibit a powerful NMDA-mediated synaptic excitation. Neurosci Lett 149:35–39.
Jones RS, Heinemann U (1988) Synaptic and intrinsic responses of medical entorhinal cortical cells in normal and magnesium-free medium in vitro. J Neurophysiol 59:1476–1496.
Kapfer C, Glickfeld LL, Atallah BV, Scanziani M (2007) Supralinear increase of recurrent inhibition during sparse activity in the somatosensory cortex. Nat Neurosci 10:743–753.
Kawaguchi Y, Kubota Y (1997) GABAergic cell subtypes and their synaptic connections in rat frontal cortex. Cereb Cortex 7:476–486.
Kawaguchi Y, Katsumaru H, Kosaka T, Heizmann CW, Hama K (1987) Fast spiking cells in rat hippocampus (CA1 region) contain the calcium-binding protein parvalbumin. Brain Res 416:369–374.
Klausberger T, Magill PJ, Márton LF, Roberts JD, Cobden PM, Buzsáki G, Somogyi P (2003) Brain-state- and cell-type-specific firing of hippocampal interneurons in vivo. Nature 421:844–848.
Klink R, Alonso A (1997) Morphological characteristics of layer II projection neurons in the rat medial entorhinal cortex. Hippocampus 7:571–583.
Kubota Y, Shigematsu N, Karube F, Sekigawa A, Kato S, Yamaguchi N, Hirai Y, Morishima M, Kawaguchi Y (2011) Selective coexpression of multiple chemical markers defines discrete populations of neocortical GABAergic neurons. Cereb Cortex 21:1803–1817.
Lee S, Hjerling-Leffler J, Zagha E, Fishell G, Rudy B (2010) The largest group of superficial neocortical GABAergic interneurons expresses ionotropic serotonin receptors. J Neurosci 30:16796–16808.
Levy RB, Reyes AD (2012) Spatial profile of excitatory and inhibitory synaptic connectivity in mouse primary auditory cortex. J Neurosci 32:5609–5619.
Lopes da Silva FH, Witter MP, Boeijinga PH, Lohman AH (1990) Anatomic organization and physiology of the limbic cortex. Physiol Rev 70:453–511.
Mainen ZF, Sejnowski TJ (1995) Reliability of spike timing in neocortical neurons. Science 268:1503–1506.
Marin-Padilla M (1969) Origin of the pericellular baskets of the pyramidal cells of the human motor cortex: a Golgi study. Brain Res 14:633–646.
McCormick DA, Connors BW, Lighthall JW, Prince DA (1985) Comparative electrophysiology of pyramidal and sparsely spiny stellate neurons of the neocortex. J Neurophysiol 54:782–806.
McCormick DA, Shu Y, Hasenstaub A, Sanchez-Vives M, Badoual M, Bal T (2003) Persistent cortical activity: mechanisms of generation and effects on neuronal excitability. Cereb Cortex 13:1219–1231.
McGarry LM, Packer AM, Fino E, Nikolenko V, Sippy T, Yuste R (2010) Quantitative classification of somatostatin-positive neocortical interneurons identifies three interneuron subtypes. Front Neural Circuits 4:12.
Miettinen M, Koivisto E, Riekkinen P, Miettinen R (1996) Coexistence of parvalbumin and GABA in nonpyramidal neurons of the rat entorhinal cortex. Brain Res 706:113–122.
Nathan T, Jensen MS, Lambert JD (1990) The slow inhibitory postsynaptic potential in rat hippocampal CA1 neurones is blocked by intracellular injection of QX-314. Neurosci Lett 110:309–313.
Oliva AA Jr, Jiang M, Lam T, Smith KL, Swann JW (2000) Novel hippocampal interneuronal subtypes identified using transgenic mice that express green fluorescent protein in GABAergic interneurons. J Neurosci 20:3354–3368.
Packer AM, Yuste R (2011) Dense, unspecific connectivity of neocortical parvalbumin-positive interneurons: a canonical microcircuit for inhibition? J Neurosci 31:13260–13271.
Petersen CC, Hahn TT, Mehta M, Grinvald A, Sakmann B (2003) Interaction of sensory responses with spontaneous depolarization in layer 2/3 barrel cortex. Proc Natl Acad Sci U S A 100:13638–13643.
Reyes A, Lujan R, Rozov A, Burnashev N, Somogyi P, Sakmann B (1998) Target-cell-specific facilitation and depression in neocortical circuits. Nat Neurosci 1:279–285.
Rudy B, Fishell G, Lee S, Hjerling-Leffler J (2011) Three groups of interneurons account for nearly 100% of neocortical GABAergic neurons. Dev Neurobiol 71:45–61.
Sanchez-Vives MV, McCormick DA (2000) Cellular and network mechanisms of rhythmic recurrent activity in neocortex. Nat Neurosci 3:1027–1034.
Schwindt PC, Spain WJ, Foehring RC, Chubb MC, Crill WE (1988) Slow conductances in neurons from cat sensorimotor cortex in vitro and their role in slow excitability changes. J Neurophysiol 59:450–467.
Shadlen MN, Newsome WT (1994) Noise, neural codes and cortical organization. Curr Opin Neurobiol 4:569–579.
Shu Y, Hasenstaub A, McCormick DA (2003) Turning on and off recurrent balanced cortical activity. Nature 423:288–293.
Siddiq A, Miyazaki T, Takagishi Y, Kanou Y, Hayasaka S, Inouye M, Seo H, Murata Y (2001) Expression of ZAKI-4 messenger ribonucleic acid in the brain during rat development and the effect of hypothyroidism. Endocrinology 142:1752–1759.
Silberberg G, Markram H (2007) Disynaptic inhibition between neocortical pyramidal cells mediated by Martinotti cells. Neuron 53:735–746.
Steriade M, Nuñez A, Amzica F (1993) A novel slow (<1 Hz) oscillation of neocortical neurons *in vivo*: depolarizing and hyperpolarizing components. J Neurosci 13:3252–3265.
Steriade M, Timofeev I, Grenier F (2001) Natural waking and sleep states: a view from inside neocortical neurons. J Neurophysiol 85:1969–1985.
Tahvildari B, Alonso A (2005) Morphological and electrophysiological properties of lateral entorhinal cortex layers II and III principal neurons. J Comp Neurol 491:123–140.
Taniguchi H, He M, Wu P, Kim S, Paik R, Sugino K, Kvitsiani D, Kvitsani D, Fu Y, Lu J, Lin Y, Miyoshi G, Shima Y, Fishell G, Nelson SB, Huang ZJ (2011) A resource of Cre driver lines for genetic targeting of GABAergic neurons in cerebral cortex. Neuron 71:995–1013.
Thomson AM, Lamy C (2007) Functional maps of neocortical local circuitry. Front Neurosci 1:19–42.
Traub RD, Whittington MA, Stanford IM, Jefferys JG (1996) A mechanism for generation of long-range synchronous fast oscillations in the cortex. Nature 383:621–624.
Tricoire L, Pelkey KA, Daw MI, Sousa VH, Miyoshi G, Jeffries B, Cauli B, Fishell G, McBain CJ (2010) Common origins of hippocampal Ivy

and nitric oxide synthase expressing neurogliaform cells. J Neurosci 30:2165–2176.

Uematsu M, Hirai Y, Karube F, Ebihara S, Kato M, Abe K, Obata K, Yoshida S, Hirabayashi M, Yanagawa Y, Kawaguchi Y (2008) Quantitative chemical composition of cortical GABAergic neurons revealed in transgenic venus-expressing rats. Cereb Cortex 18:315–330.

van den Pol AN, Yao Y, Fu LY, Foo K, Huang H, Coppari R, Lowell BB, Broberger C (2009) Neuromedin B and gastrin-releasing peptide excite arcuate nucleus neuropeptide Y neurons in a novel transgenic mouse expressing strong *Renilla* green fluorescent protein in NPY neurons. J Neurosci 29:4622–4639.

Wang XJ (2001) Synaptic reverberation underlying mnemonic persistent activity. Trends Neurosci 24:455–463.

Wehr M, Zador AM (2003) Balanced inhibition underlies tuning and sharpens spike timing in auditory cortex. Nature 426:442–446.

Witter MP, Groenewegen HJ, Lopes da Silva FH, Lohman AH (1989) Functional organization of the extrinsic and intrinsic circuitry of the parahippocampal region. Prog Neurobiol 33:161–253.

Xu X, Roby KD, Callaway EM (2006) Mouse cortical inhibitory neuron type that coexpresses somatostatin and calretinin. J Comp Neurol 499:144–160.

Xu X, Roby KD, Callaway EM (2010) Immunochemical characterization of inhibitory mouse cortical neurons: three chemically distinct classes of inhibitory cells. J Comp Neurol 518:389–404.

Yu Y, Hill AP, McCormick DA (2012) Warm body temperature facilitates energy efficient cortical action potentials. PLoS Comput Biol 8:e1002456.

Zhang ET, Hansen AJ, Wieloch T, Lauritzen M (1990) Influence of MK-801 on brain extracellular calcium and potassium activities in severe hypoglycemia. J Cereb Blood Flow Metab 10:136–139.